Regional Studies in Marine Science 101 (2026) 105231

Contents lists available at ScienceDirect

Regional Studies in Marine Science

journal homepage: www.elsevier.com/locate/rsma

Three decades of shoreline dynamics in the northern Persian Gulf: A multi-estuary assessment using Landsat, MNDWI, and DSAS metrics

Shiva Rastgou [a], Hana Etemadi [b,*], Esmaeil Abbasi [b,*], Hamid Amoonia [c]

[a] Department of Biological Science and Technology, Nano and Bio Science and Technology, Persian Gulf University, Bushehr, Iran
[b] Environmental Science Department, Persian Gulf Research Institute, Persian Gulf University, Bushehr, Iran
[c] Department of Geography Education, Farhangian University, P.O. Box 14665-889, Tehran, Iran

ARTICLE INFO

Keywords:
Shoreline change detection
Geographic Information System (GIS)
Persian Gulf
Landsat imagery

ABSTRACT

Coastal estuaries are among the most dynamic and ecologically sensitive environments, yet they are increasingly threatened by anthropogenic activities and climate-related stressors. This study investigates three decades (1990–2020) of shoreline dynamics in three major estuaries along the northern Persian Gulf—Bidkhoon, Ziarat, and Shif—each exhibiting distinct morphodynamic characteristics and varying degrees of human influence. Using multi-temporal Landsat imagery within a GIS environment, shoreline positions were extracted using the Modified Normalized Difference Water Index (MNDWI) and analyzed with the Digital Shoreline Analysis System (DSAS). Shoreline change was quantified using the Net Shoreline Movement (NSM) and Linear Regression Rate (LRR) metrics. Mean LRR values of −1.4, −9.02, and −25.2 m yr^{-1} were estimated for the Bidkhoon, Ziarat, and Shif estuaries, respectively. Bidkhoon, which lacks significant fluvial sediment input, exhibited a predominantly erosional shoreline with relatively low spatial variability, suggesting a largely tide-dominated coastal system. Shif experienced the largest absolute shoreline fluctuations (maximum NSM erosion: −2332.17 m; maximum accretion: +1326.85 m) and displayed a complex pattern of alternating erosion and accretion, with localized retreat within the Helleh River delta and shoreline progradation elsewhere, likely associated with aquaculture development and sediment redistribution. Ziarat exhibited the most pronounced shoreline retreat, reaching a maximum NSM of −989.86 m, consistent with reduced sediment supply following the construction of the Salman Dam. Regional relative sea-level rise and land subsidence may have further contributed to shoreline retreat, particularly within the Mond River delta. Although all three estuaries are located within protected coastal areas characterized by limited urban and industrial development, the observed shoreline changes demonstrate that both natural coastal processes and human activities have substantially influenced estuarine evolution over the past three decades. These findings provide valuable information for understanding long-term shoreline dynamics and support the development of sustainable coastal management strategies for the northern Persian Gulf.

1. Introduction

Coastal ecosystems rank among the world's most productive systems, offering essential goods and services for humankind. They are distinctive and ecologically diverse regions, serving as a highly suitable habitat for various animal and plant species (Crain et al.,2009; Etemadi et al., 2016). They are also the world's most densely populated regions, which possess unique conditions encompassing economic, commercial, recreational, and, in some cases, strategic aspects (Harley et al., 2006). Therefore, coastal zones hold enormous social, economic, and biological value (Martínez et al., 2007). Also, the coasts represent the most dynamic zones found at the interface of land, water, and the atmosphere, making them susceptible to human activities such as tourism, offshore oil and gas operations, port activities, fisheries, and navigation (Etemadi et al., 2018) Additionally, natural processes like inundation or erosion due to sea level rise, storms, cyclones, hurricanes, and tsunamis pose significant challenges to them (Abbasi et al., 2021). Numerous processes and factors such as the intensity of wave energy incident upon the shoreline, changes in sea level, local tectonic activity, sediment availability, coastal geomorphology, and fluvial flow—interact in a complex manner to define both the shape and alignment of the shore (Hecht and Cordeira, 2017).

* Corresponding authors.
E-mail addresses: h.etemadi@pgu.ac.ir (H. Etemadi), esmaeil.abbasi@pgu.ac.ir (E. Abbasi).

https://doi.org/10.1016/j.rsma.2026.105231
Received 18 November 2025; Received in revised form 7 July 2026; Accepted 8 July 2026
Available online 10 July 2026

Coastal erosion poses a major environmental threat, especially in low-lying coastal regions, and is a critical concern for coastal developers (Crowell et al., 1991). Erosion is defined as the landward retreat caused by sediment loss, while accretion refers to seaward advance due to sediment gain (Mills et al., 2005). This process directly results in land loss and the submergence of infrastructure, agricultural land, and beaches (Williams et al., 2018). Continuous coastal erosion negatively affects the livelihoods of coastal populations (Mukhopadhyay et al., 2018) and drives the loss of habitable land, mangroves, farmland, and other natural and anthropogenic resources (Mondal et al., 2020). In recent decades, net erosion has been observed on over 70% of the world's sandy beaches, underscoring coastal erosion as a persistent issue in coastal zone management (Melet et al., 2020).

Monitoring coastline changes is pivotal for sustainable development and the environmental protection of coastal ecosystems (Hossain et al., 2022b). Spatiotemporal observations of coastal areas enable the assessment of erosion risk and the detection of change patterns. Such monitoring also supplies essential data to guide the development of intervention policies when needed (Appeaning Addo et al., 2008). Coastal areas' vulnerability to these hazards, combined with limited adaptive capacity, highlights the increasing need for sustained monitoring, understanding, and forecasting of marine coastal hazards. To reduce risks associated with marine hazards, enhanced coastal zone monitoring and forecasting programs are urgently required (Hossain et al., 2022a; Mondal et al., 2025; Das et al., 2025). Sustainable coastal management necessitates viewing the coastal zone as a system, with the ability to both reconstruct past shoreline changes and project future changes across multiple timeframes (Davidson et al., 2010; Miller and Dean, 2004; Mondal et al., 2020). Consequently, accurate shoreline delineation and continuous monitoring are essential for implementing remedial measures—including afforestation, sea walls, and dykes—to counter these alterations.

Accurate delineation and long-term monitoring of shoreline position are fundamental for understanding coastal evolution and supporting sustainable coastal management (Alesheikh et al., 2007; Nassar et al., 2018; Mondal et al., 2017). Among the available approaches, satellite remote sensing has become one of the most reliable and cost-effective techniques for investigating shoreline dynamics because it provides extensive spatial coverage, long-term historical archives, high temporal revisit capability, and multispectral information suitable for land–water discrimination (Zhang et al., 2017; Gunasegaram et al., 2022). Optical satellite imagery is particularly effective for shoreline mapping because water strongly absorbs near-infrared radiation, whereas vegetation and exposed land surfaces exhibit relatively high reflectance. Consequently, spectral water indices derived from visible and infrared bands, such as the Modified Normalized Difference Water Index (MNDWI), have been widely applied to extract shoreline positions with improved accuracy under different coastal conditions (Alesheikh et al., 2007). Following shoreline extraction, shoreline change can be quantified using statistical indicators such as the End Point Rate (EPR), Linear Regression Rate (LRR), Net Shoreline Movement (NSM), and Shoreline Change Envelope (SCE), which enable robust evaluation of long-term erosion and accretion trends.

The Digital Shoreline Analysis System (DSAS) is one of the most widely adopted tools for calculating shoreline change statistics from multi-temporal shoreline datasets (Moore, 2000; Thieler et al., 2009; Bera and Maiti, 2019; Jodhani et al., 2021). Integrated with Geographic Information Systems (GIS), DSAS provides standardized and reproducible estimates of shoreline movement, allowing comparison of shoreline dynamics across different spatial and temporal scales. Owing to its reliability and operational efficiency, DSAS has been successfully applied to a wide variety of coastal environments worldwide, including sandy beaches, estuaries, deltas, and embayed coastlines in Africa, Asia, Europe, and Australia (Mukhopadhyay et al., 2012; Moussaid et al., 2015; Kermani et al., 2016; Jonah et al., 2016; Hakko et al., 2018; Ataol et al., 2019; Konlechner et al., 2020; Thakur et al., 2020b; Gormüs et al., 2021; Mishra et al., 2024b; Paul et al., 2025). These studies collectively demonstrate the effectiveness of integrating satellite remote sensing and DSAS for evaluating long-term shoreline dynamics while emphasizing that shoreline responses remain highly site-specific because they are controlled by local geomorphological and hydrodynamic conditions.

In Iran, previous studies have applied remote sensing and DSAS to investigate shoreline changes along several sectors of the Persian Gulf and the Strait of Hormuz (Razmi et al., 2018; Parhizkar et al., 2019). Previous coastal investigations have documented considerable spatial variability in shoreline behaviour between 1976 and 2018, with some sectors remaining relatively stable, others experiencing shoreline retreat, and others exhibiting progressive sediment accumulation (Sotoudepour et al., 2020).

However, comprehensive long-term assessments focusing on the major estuaries along the northern Persian Gulf remain limited, despite their ecological significance and increasing socioeconomic importance. Estuaries are among the most dynamic and environmentally significant components of coastal systems, where the interaction of river discharge, tidal processes, waves, and sediment transport controls shoreline morphology and estuarine stability. Owing to their ecological, economic, and strategic importance, understanding long-term shoreline dynamics within estuarine environments is essential for sustainable coastal management and effective planning of coastal infrastructure. Along the southern coast of Iran, rapid coastal development, including the construction of ports, breakwaters, and other coastal engineering structures, has the potential to modify local hydrodynamic conditions and sediment transport processes. Although these activities are considered possible drivers of shoreline evolution, their influence varies spatially depending on local geomorphological and environmental conditions (Naeimi et al., 2010).

Despite the regional importance of the major estuaries along the northern Persian Gulf, omprehensive long-term assessments of shoreline dynamics within these estuarine systems remain limited. Most previous investigations have focused on broader coastal sectors, leaving significant uncertainty regarding the spatial variability of erosion and accretion in the largest estuaries of Bushehr Province. This knowledge gap limits the development of effective management strategies for these environmentally sensitive and strategically important coastal environments. This study investigates the long-term shoreline dynamics of the three largest estuaries in Bushehr Province Bidekhoon, Ziarat, and Shif—using multi-temporal Landsat imagery acquired in 1990, 2000, 2010, and 2020 together with the Modified Normalized Difference Water Index (MNDWI) and the Digital Shoreline Analysis System (DSAS). Beyond quantifying shoreline change rates, this study evaluates the spatial variability of erosion and accretion among the major estuarine systems and provides a regional baseline for future coastal monitoring and management in the northern Persian Gulf. Although the methodological framework is based on well-established remote sensing techniques, the scientific contribution of this study lies in improving the understanding of long-term shoreline behaviour within the largest estuaries of the northern Persian Gulf, where comparable investigations remain scarce despite their ecological and socioeconomic importance. These largest estuaries are located within or adjacent to nationally protected coastal ecosystems and marine conservation areas. These estuaries represent environmentally sensitive habitats that support valuable wetlands, mangroves, and diverse aquatic communities making the assessment of their long-term shoreline dynamics particularly important for ecosystem conservation and coastal management.

The findings also contribute to the growing body of international research employing remote sensing and DSAS to evaluate shoreline dynamics in environmentally sensitive coastal systems, while providing new evidence from the understudied estuarine environments of the northern Persian Gulf.

2. Study site

The coastal zone of Bushehr Province is located in the northern sector of the Persian Gulf, extending between 48°40' to 52°44' E and 27°17' to 30°10' N. This region encompasses a substantial portion of the Persian Gulf coastline and is characterized by diverse geomorphological features, including coastal hills, lagoons, rivers, islands, and volcanic cones.

Among the estuarine systems of Bushehr Province, the Bidkhoon, Ziarat, and Shif estuaries were selected because they are the largest and most environmentally significant estuaries along the northern Persian Gulf (Fig. 1). These estuaries differ in their geomorphological characteristics, hydrodynamic settings, and sedimentary environments, providing an opportunity to evaluate spatial variability in shoreline evolution within representative estuarine systems of the region.

The Bidkhoon Estuary extends approximately 5.25 km across the gently sloping coastal plain of eastern Asaluyeh and southern Bidkhoon District. Tidal processes support an extensive wetland covering approximately 8400 ha, which is located in Nayband national marine park, also provides habitat for numerous aquatic birds, fish species, and mangrove communities (Etemadi et al., 2021). The Ziarat Estuary is located near the mouth of the Mond River in Mond protected area, where the coastal plain has a general slope of less than 4%. Its geomorphology is strongly influenced by interactions between river discharge and tidal processes (Abbasi et al., 2024). The Shif Estuary, situated within the protected Helle coastal area, is recognized as one of the largest and most productive estuarine lagoons in the region and represents an ecologically important coastal wetland.

The climate of the study area is arid to semi-arid. Mean annual relative humidity is approximately 43%, and average annual precipitation is less than 250 mm, with nearly 60% of rainfall occurring between December and February, whereas precipitation is minimal from June to September. The prevailing northwesterly winds generate wave action and longshore currents that influence sediment transport and shoreline evolution along the coast. In addition, the region experiences a semi-diurnal tidal regime with tidal amplitudes ranging from approximately 0.5–1.5 m, reaching higher levels during the monsoon and post-monsoon periods and lower levels during summer (Iran Meteorological Organization, 2024)(http://www.irimo.ir). These climatic and oceanographic conditions collectively influence sediment redistribution and the temporal variability of shoreline position within the study area (Table 1).

3. Materials and methods

3.1. Data sources

To evaluate coastline changes along the Bushehr Province, satellite imagery from the Landsat mission was acquired for multiple temporal intervals 1990, 1995, 2000, 2005, 2010, 2014, 2015, 2019, and 2020 covering a 30-year period (Table 2). All images utilized in this study were freely downloaded in GeoTIFF format from the US Geological Survey (USGS) Earth Explorer platform (https://earthexplorer.usgs.gov).

Table 1
Tidal characteristics of studied estuaries.

Study Area	Tidal Station (Lat/Lon)	MHHW	MLHW	MHLW	MLLW	ML
Bidkhoon	27° 30', 52° 35'	1.89	1.46	0.86	0.44	1.16
Ziarat	28° 00', 51° 23'	1.9	1.51	0.83	0.46	1.17
Shif	28° 59', 50° 50'	1.87	1.31	1.11	0.55	1.21

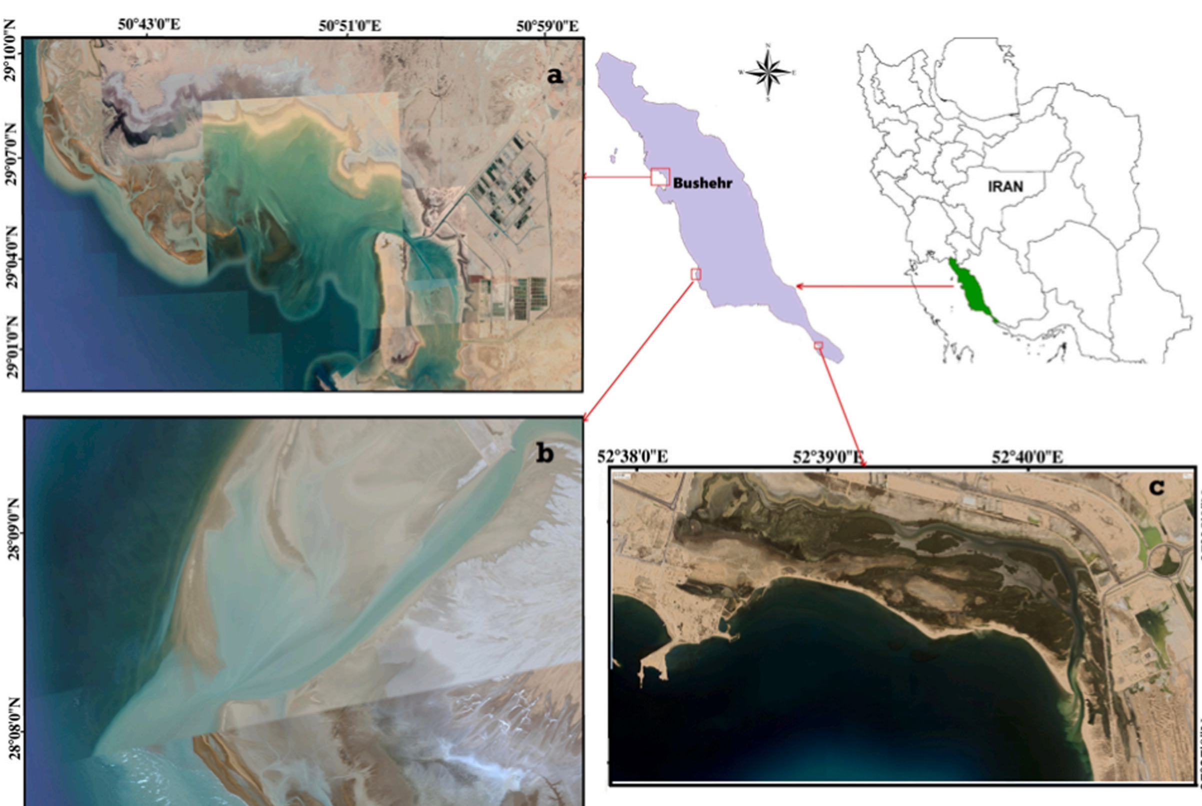

Fig. 1. The maps of the estuaries under study: a. Shif, b. Ziarat, c. Bidkhoon.

Table 2
Detailed information on the analyzed satellite images.

Study sits	Satellite/ sensor	Pixel size (m)	zone	Path/ row	Date of acquisition
Bidkhon estuary	Landsat 5/ TM	30	39	162/ 041	Jun 02, 1991
	Landsat 5/ TM	30	39	162/ 041	Jan 04, 1995
	Landsat 7/ ETM$^+$	30	39	162/ 041	Jul 04, 2000
	Landsat 7/ ETM$^+$	30	39	162/ 041	May 15, 2005
	Landsat 7/ ETM$^+$	30	39	162/ 041	Jul 16,2010
	Landsat 8/ OLI	30	39	162/ 041	Jun 17, 2014
	Landsat 8/ OLI	30	39	162/ 041	Aug 20, 2020
Ziarat estuary	Landsat 4/ TM	30	39	163/ 041	Feb 25, 1991
	Landsat 5/ TM	30	39	163/ 041	Jan 27, 1995
	Landsat 7/ ETM$^+$	30	39	163/ 041	Feb 18, 2000
	Landsat 7/ ETM$^+$	30	39	163/ 041	Feb 26, 2003
	Landsat 7/ ETM$^+$	30	39	163/ 041	Jan 28, 2010
	Landsat 8/ OLI	30	39	163/ 041	Feb 25, 2015
	Landsat 8/ OLI	30	39	163/ 041	Feb 14, 2019
Shif estuary	Landsat 7/ ETM$^+$	30	39	164/ 040	Jul 02, 2000
	Landsat 7/ ETM$^+$	30	39	164/ 040	May 19, 2007
	Landsat 7/ ETM$^+$	30	39	164/ 040	Jul 14, 2010
	Landsat 8/ OLI	30	39	164/ 040	Jul 17, 2014
	Landsat 8/ OLI	30	39	164/ 040	Sep 19, 2020

3.2. Field surveying

Ground verification was carried out through field surveys. Seventy-five Ground Control Points (GCPs) were acquired at different shoreline locations using a GPS unit (±15 m accuracy) over the period from December 2019 to January 2020.

3.3. Image processing

Image selection followed a rigorous screening process to ensure the absence of stripping defects and other radiometric anomalies. After selection, the images were geometrically aligned and clipped to the spatial extent of the study area. Subsequently, both geometric and radiometric corrections were applied. Radiometric correction is essential for minimizing atmospheric effects, particularly in the visible and near-infrared spectral bands, where atmospheric absorption can significantly influence reflectance values. Quick Atmospheric Correction (QUAC) or the FLAASH algorithm was employed to derive surface reflectance values.It is important to recognize that not all of the aforementioned corrections are universally required; preprocessing operations are conducted primarily to isolate essential spatial–spectral components and minimize potential sources of error, thereby ensuring the extraction of accurate information from satellite datasets. All images were georeferenced to the World Geodetic System 1984 (WGS84) datum using the Universal Transverse Mercator (UTM) projection and 75 GCPs. The GPS observations collected during the 2019–2020 field surveys were used as Ground Control Points (GCPs) to improve the geometric correction and co-registration of the multi-temporal Landsat imagery. The selected GCPs were permanent and spatially stable features.Following preprocessing, an appropriate vector boundary was generated for each study estuary, after which the corresponding satellite images were clipped and prepared for subsequent analytical procedures. ENVI 5.3 and ArcGIS 10.3 software packages were used for the processing, analysis, and visualization of remote-sensing datasets.

3.4. Shoreline extraction and analysis

The determination of shoreline positions utilized the high water level (HWL) proxy, a widely employed indicator for shoreline definition (Boak and Turner, 2005; Del Río and Gracia, 2012). Tidal data were obtained from the Costal Area Hydrography Management in National Cartographic Center (http://www.ncc.org.ir).

To minimize the influence of tidal variability, the satellite images were not selected solely based on their acquisition season or date. Instead, hourly tidal records from the Bushehr tidal station were used to determine the tidal stage corresponding to the exact date and satellite overpass time of each Landsat image. Images were preferentially selected when the tidal stage was close to the High Water Level (HWL), and the tidal levels for all selected images were verified to be comparable across the study period. This approach ensured that the extracted shorelines represented similar tidal conditions, thereby reducing uncertainties associated with tidal fluctuations, particularly along the low-gradient estuarine coastlines of the study area, where even small differences in tidal elevation can result in substantial horizontal shifts in shoreline position.

Although the images were acquired in different years, seasonal consistency was maintained as far as possible within each estuary. Specifically, all images for the Ziarat Estuary were acquired during January–February, most images for the Bidkhoon Estuary during May–August, and all images for the Shif Estuary during May–September. Where identical seasonal imagery was unavailable, image selection prioritized comparable High Water Level (HWL) conditions to minimize tidal-induced shoreline variability.

To distinguish between water and land boundaries, the Modified Normalized Difference Water Index (MNDWI) (Eq1)

$$\text{MNDWI}=\text{Green}-\text{SWIR}/\text{Green}+\text{SWIR} \tag{1}$$

where "Green" and short-wave infrared "SWIR" represent reflectance values in the green and SWIR bands, This modification effectively suppresses built-up land, vegetation, and soil noise, providing clearer delineation of water bodies in satellite imagery such as Landsat and Sentinel−2 data. MNDWI values typically range from –1–1, with higher values indicating water presence. It is recognized as one of the best indices for delineating water boundaries (Fig. 2) among the spectral indices and were calculated using ENVI 10.5 software (Salehipour Milani, Eskansari, 2021). Because the spectral characteristics of the satellite images varied among acquisition dates, a single threshold could not be applied to all images. Therefore, the MNDWI threshold was determined individually for each image through an iterative visual procedure in ENVI. Several threshold values were tested for each image, and the resulting land water boundaries were visually evaluated to identify the threshold that provided the most realistic shoreline. The selected shoreline was subsequently compared with the corresponding high resolution Google Earth imagery available for approximately the same period to verify its consistency with the actual land water boundary before proceeding to edge detection.

Edge detection is a fundamental process in object recognition, aiming to identify sharp discontinuities in image intensity that define object boundaries, ultimately producing a line drawing representation of the input image. Among various edge detection techniques, the Canny operator stands out as the most effective and widely used method, particularly for applications such as shoreline extraction from remote sensing imagery. The Canny algorithm employs a multi-stage approach:

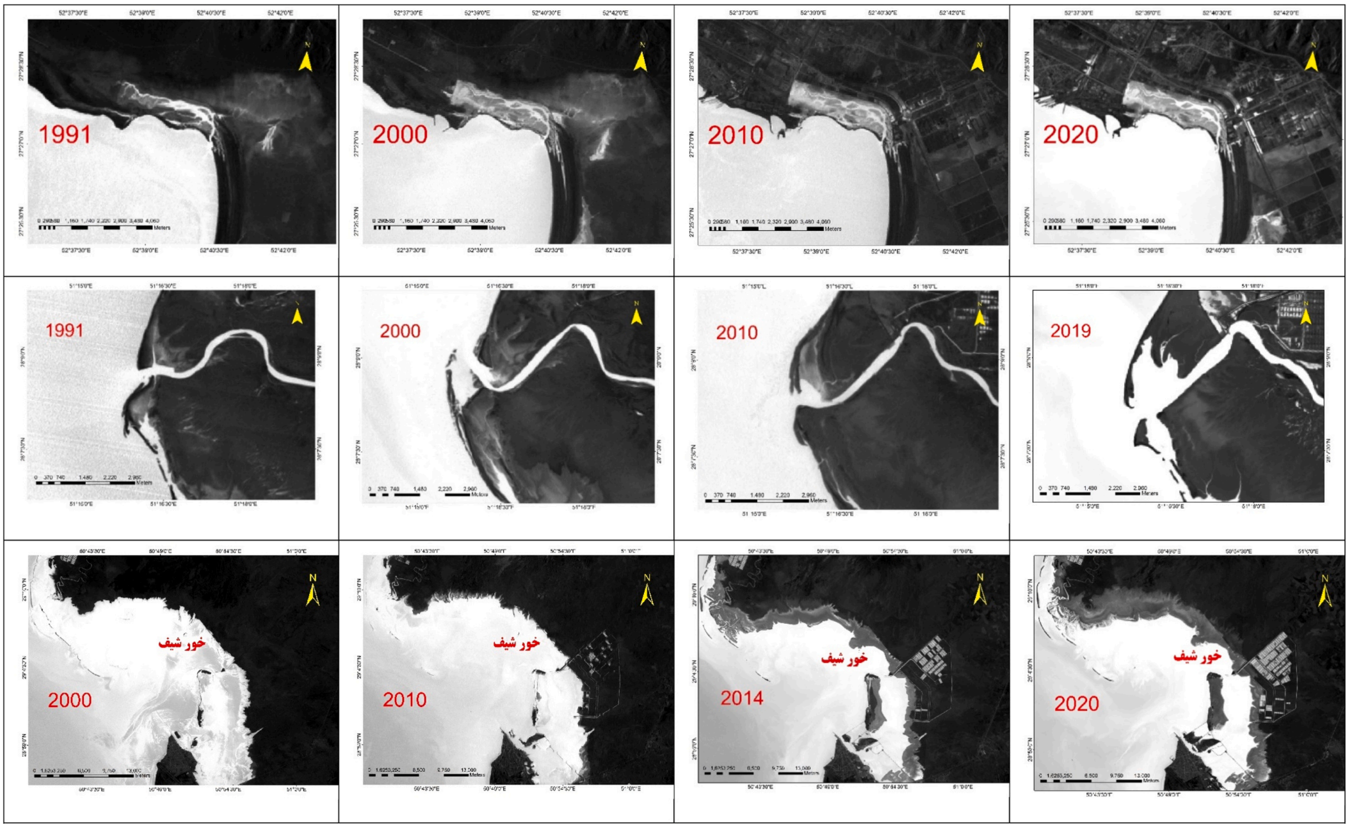

Fig. 2. Shoreline extraction by MNDWI and in Bidkhoon (firest row), Ziarat (scound row), Shif estuary (third row) (just select 4years in each site). It illustrate the quality of the land–water separation using the selected spectral index and estuary shoreline change during long period of time.

it begins with Gaussian smoothing to reduce noise, followed by gradient calculation (often using Sobel kernels) to determine intensity changes, non-maximum suppression to thin the edges, and double thresholding with hysteresis to robustly identify true edges. In satellite images, where the transition between land and sea is marked by step-like changes in grayscale values, the Canny operator excels in accurately delineating coastal boundaries with minimal breakpoints and high continuity. In this study, the Canny edge detector implemented in ENVI was applied using the software's default processing parameters, including Gaussian smoothing and hysteresis threshold settings. These default parameters provided continuous shoreline boundaries with minimal edge discontinuities across all study areas and therefore were retained for all images to ensure methodological consistency. The mathematical formulation (Eq. 2) for the gradient magnitude in the Canny edge detector is:

$$G = \sqrt{G_x^2 + G_y^2} \tag{2}$$

where G_xG_x and G_yG_y are the gradients in the x and y directions, respectively. This optimized approach ensures precise edge positioning and reliable extraction of well-defined image features, making Canny the preferred choice for high-quality edge detection in remote sensing applications.

3.5. DSAS analysis

After extracting shoreline lines, shoreline change rates are determined using DSAS software's End Point Rate (EPR), NSM (Net Shoreline Movement) and Linear Regression Rate (LRR) techniques over 30 years. This software calculates the amount of shoreline movement and changes in each period by applying a perpendicular transect to the shoreline and using a baseline. To capture diverse developmental changes and microhabitats along the shoreline within short distances, shore-parallel baselines were established.

The extracted shoreline vectors were subsequently imported into the DSAS to quantify shoreline changes over the study period. After shoreline extraction, a landward buffer was generated from each shoreline to construct the DSAS baseline. The baseline was positioned inland and approximately parallel to the general shoreline orientation to avoid intersection with the extracted shoreline positions while ensuring that all shorelines could be intersected by the generated transects. Transects were automatically generated from the baseline using the DSAS extension. All transects were created perpendicular to the baseline at regular intervals to provide consistent measurements of shoreline displacement throughout the study area. A transect spacing of 100 m was adopted as a compromise between capturing local shoreline variability and maintaining a manageable number of measurement locations. This interval was considered sufficient to represent shoreline changes while avoiding excessive redundancy among adjacent transects.

After creating feature classes for each section, the percentage of Net Shoreline Movement) and SCE (Shoreline Change Envelope) (Ayadi, et al., 2016). Qualitative analysis was also performed to determine erosion/sedimentation sections using the NSM model, which represents the net distance between the old and new shoreline positions for each segment. Negative values of NSM, LRR, EPR, and SCE indicate shoreline retreat, while positive values indicate shoreline accretion. The calculation method for LRR is as follows: the rate of shoreline changes is obtained by fitting a least-squares regression line to all shoreline lines within a transect (Temitopi and Oyedotun, 2014; Thieler, et al., 2009). In the next step, the maps of shoreline change were classified again in the ArcGIS software to visualize the trend of changes in the shoreline over 30 years.The executable steps of the research are presented in the flowchart below (Fig. 3).

The accuracy of the MNDWI-based shoreline extraction was evaluated using 200 stratified random validation samples generated

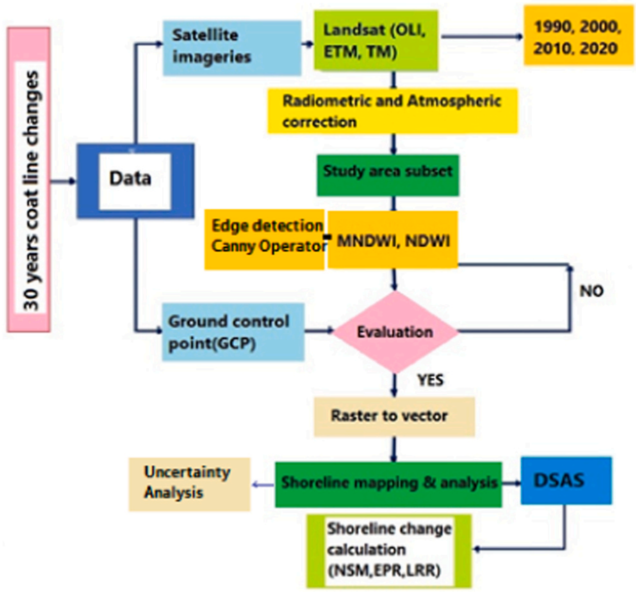

Fig. 3. Flowchart of the data processing procedure used in this study.

independently for each estuary. The validation samples were randomly distributed over the land and water classes in the MNDWI-derived maps and their reference classes were identified through visual interpretation of high-resolution Google Earth imagery together with field observations. Confusion matrices were constructed by comparing the classified land and water classes with the corresponding reference data for each study site (Table 3). Based on the confusion matrices, Overall Accuracy (OA), User's Accuracy (UA), Producer's Accuracy (PA), and the Kappa coefficient (κ) were calculated to evaluate the reliability of the extracted shorelines (Table 4). When the obtained classification accuracy was considered unsatisfactory, the MNDWI threshold was refined through the iterative threshold optimization procedure described in the previous section before converting the classified raster to shoreline vectors for subsequent DSAS analysis. This iterative procedure ensured that the selected threshold produced the highest agreement between the extracted shoreline and the reference shoreline before shoreline vectorization.

3.6. Uncertainty analysis

Accurate shoreline extraction from multi-temporal satellite imagery is affected by several sources of uncertainty associated with image characteristics, shoreline delineation, tidal conditions, seasonal variability, and geometric registration (Jonah et al., 2016; Vu et al., 2020). To evaluate the reliability of the extracted shorelines, a comprehensive uncertainty assessment was performed following the approach proposed by Hapke et al. (2010) and Gopinath et al. (2023). This assessment provides a quantitative measure of shoreline positional uncertainty and facilitates a more reliable interpretation of long-term shoreline change patterns.

Table 3
Confusion matrices for the accuracy assessment of MNDWI-based shoreline extraction in the three study estuaries.

Study site	Reference Data	Water	Land	Total
Bidkhon estuary	Water	88	12	100
	Land	14	86	100
	Total	102	98	200
Shif estuary	Water	84	16	100
	Land	17	83	100
	Total	101	99	200
Ziarat estuary	Water	82	18	100
	Land	22	78	100
	Total	104	96	200

Three principal sources of positional uncertainty were considered in the calculation of shoreline position uncertainty: georeferencing uncertainty (Ug), shoreline digitization uncertainty (Ud), and uncertainty associated with the high water level (HWL) shoreline proxy (Uhwl). Georeferencing uncertainty reflects residual geometric registration errors among the multi-temporal Landsat images, digitization uncertainty represents errors introduced during shoreline delineation, and HWL uncertainty accounts for positional variation associated with the selected shoreline indicator. Following Hapke et al. (2010), the total shoreline position uncertainty for each acquisition year was calculated as: Eq. (3)

$$\sqrt{U_g^2 + U_d^2 + U_{hwl}^2} \quad (3)$$

.

Additional measures were implemented to minimize other potential sources of uncertainty. To reduce tidal uncertainty, hourly tidal observations from the Bushehr tidal station were used to determine the tidal stage at the exact Landsat overpass time. Images were preferentially selected under comparable High Water Level (HWL) conditions, thereby substantially reducing shoreline displacement caused by tidal fluctuations.

Seasonal uncertainty was also minimized through the image selection strategy. Although the satellite images were acquired over different years, seasonal consistency was maintained as far as possible within each estuary. Specifically, all images used for the Ziarat Estuary were acquired during January–February, most images for the Bidkhun Estuary during May–August, and all images for the Shif Estuary during May–September. Furthermore, the study area is located in an arid coastal environment with relatively limited seasonal freshwater inflow, particularly in the Bidkhun Estuary, which lacks a permanent river discharge. Consequently, seasonal effects on shoreline position are expected to be smaller than tidal influences. Nevertheless, seasonal variability remains a potential source of residual uncertainty and is acknowledged as a limitation of this study.

Sensor-related uncertainty was further reduced by employing Landsat TM, ETM+, and OLI imagery with a consistent spatial resolution of 30 m. All images underwent identical geometric and radiometric preprocessing and were co-registered to the WGS84/UTM coordinate system using 75 GPS-derived Ground Control Points (GCPs) located on permanent and spatially stable features. This procedure minimized positional inconsistencies among sensors acquired over the 30-year study period. The calculated total shoreline uncertainties for each study year are presented in Table 5.

4. Results

4.1. Shoreline dynamics in the Bidkhoon estuary

The Bidkhoon estuary, located within Nayband National Park, has undergone notable morphological adjustments over the past three decades. Using cloud-free Landsat images acquired during peak high-tide conditions, shoreline variations were assessed across five geomorphic sectors (A–E) (Fig. 4). In Area A, located near the estuarine inlet, the shoreline exhibited continuous landward advancement throughout the study period. Prior to 2000, the shoreline retreated inland, and between 2000 and 2014, erosion persisted with maximum annual advancement and retreat values of 5.34 m and 53.39 m, respectively. Area B demonstrated relative stability, as reflected by low LRR values and NSM values ranging between −22.39 m and +13.93 m, with portions showing no measurable change. In Area C, erosion was most pronounced, with maximum retreat reaching −147.6 m (NSM) and a peak annual displacement of −5.17 m yr^{-1} (LRR). Area D also showed shoreline retreat, though with smaller LRR magnitudes. NSM indicated a

Table 4
Overall Accuracy (OA), Kappa coefficient (k), User's Accuracy (UA), and Producer's Accuracy (PA) for shoreline extraction in the study estuaries.

Study site	Validation samples	OA (%)	Kappa (κ)	Water UA (%)	Water PA (%)	Land UA (%)	Land PA (%)
Bidkhon estuary	200	87.0	0.74	86.3	88.0	87.8	86.0
Shif estuary	200	80.0	0.60	78.8	82.0	81.3	78.0
Ziarat estuary	200	83.5	0.67	83.2	84.0	83.8	83.0

Table 5
Total shoreline position uncertinity (m) in each year.

Study sits	Total Uncertinity	year
Bidkhon estuary	10.24	1991
	8.1	1995
	6.3	2000
	8.5	2005
	5	2010
	5.6	2014
	4.5	2020
Ziarat estuary	9.75	1991
	10.5	1995
	8.2	2000
	7	2003
	6.7	2010
	7.1	2015
	5.3	2019
Shif estuary	8.1	2000
	9	2007
	6.8	2010
	5	2014
	4.1	2020

maximum landward shift of −51.84 m. In Area E, morphological changes intensified following construction activities after 2010. Erosion dominated (LRR = −5.58 m yr^{-1}), with maximum NSM retreat reaching −121.49 m Figs. 5 and 6 show NSM and Figs. 7 and 8 show LRR in the Bidkhoon estuary. Collectively, the Bidkhoon estuary exhibited a predominantly erosional trend, with localized influences from hydrodynamic forcing and construction activities.

4.2. Shoreline dynamics in the Ziarat estuary

The Ziarat estuary, positioned at the mouth of the Mond River (Fig. 9), underwent the most substantial shoreline transformations among the three estuaries. Over a 28-year interval (1991–2019), changes in river course, aquaculture expansion, artificial channeling, and sea-level fluctuations substantially modified the shoreline. In Area A, the shoreline largely advanced seaward due to aquaculture development. Maximum NSM accretion reached +347 m, with an LRR rate of 19 m yr^{-1} . Area B showed high instability, characterized by maximum accretion of +503 m and maximum erosion of −328 m. LRR values ranged between +14 m yr^{-1} and −12.25 m yr^{-1} . In Area C, the longitudinal and transverse shifts of the Mond River caused shoreline readjustments. Maximum NSM advancement was +396 m, while erosion

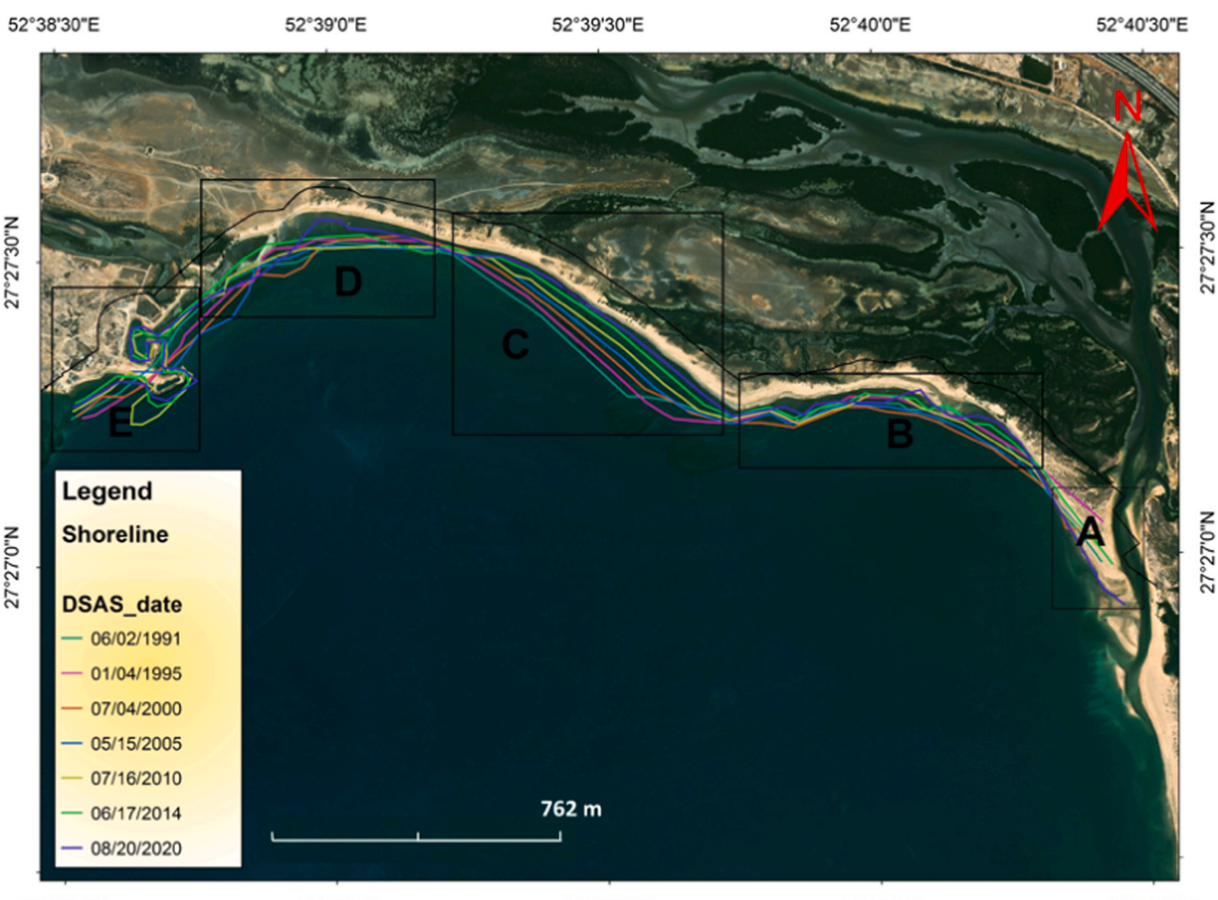

Fig. 4. Shoreline extraction using MNDWI on Landsat imagery along the Bidkhoon estuary (1990–2020), The line colors show the date of shoreline extraction, This coastline was segmented into five (A,B,C,D,E) distinct zones.

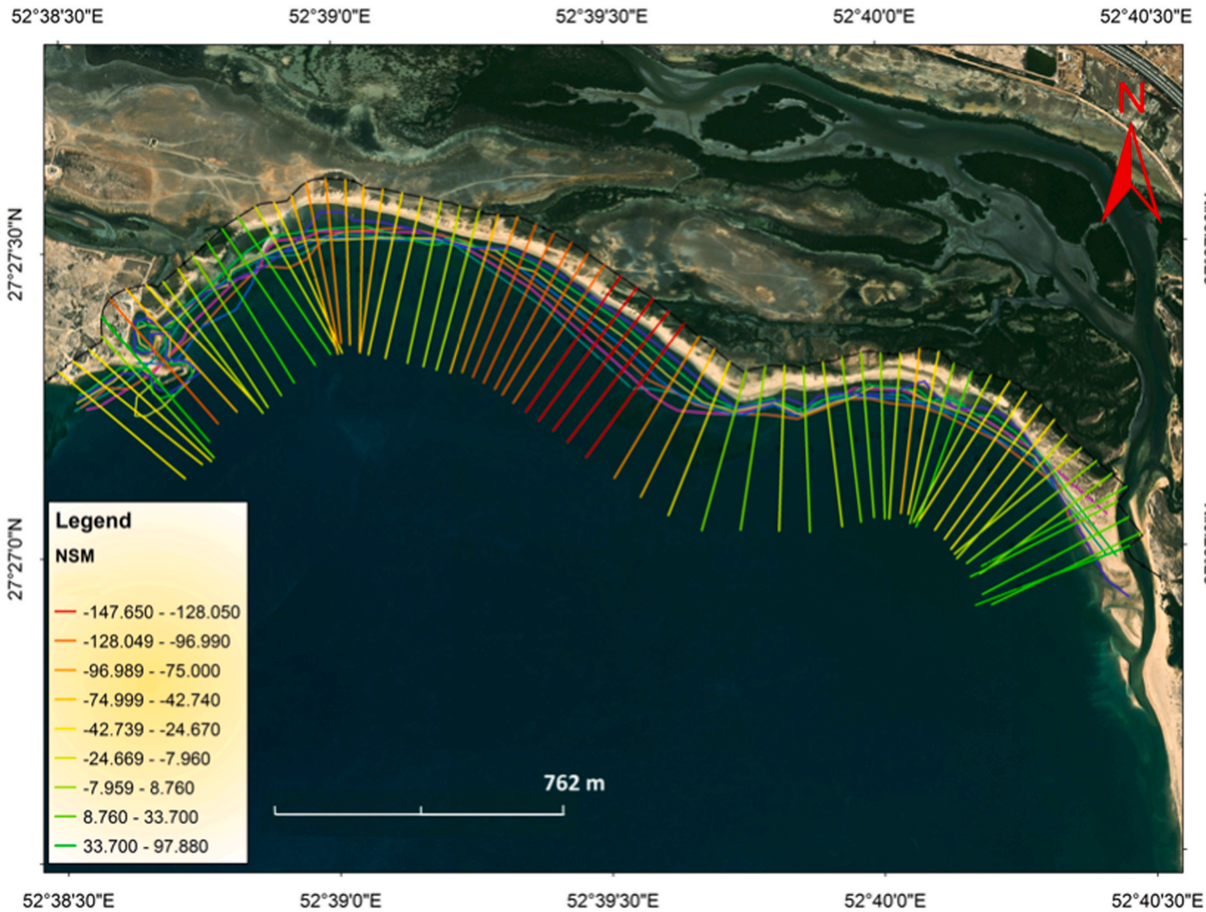

Fig. 5. Shoreline change (1990–2020) using the Net shoreline changes (NSM) (m) along the Bidkhoon estuary.

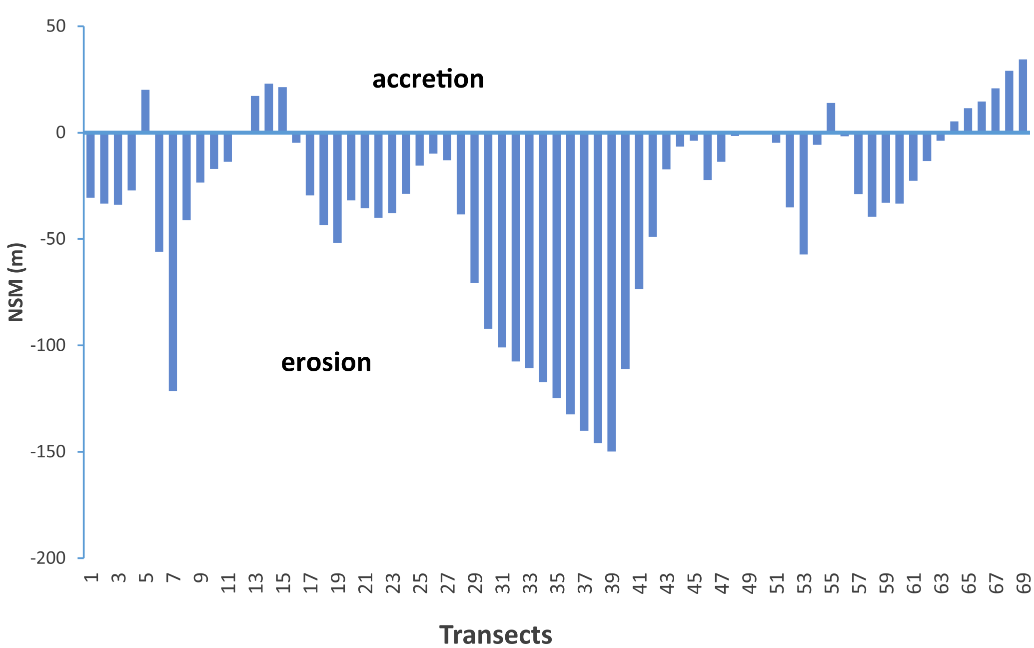

Fig. 6. Net shoreline changes (NSM) (m), shoreline accretion and erosion along the Bidkhoon estuary (1990–2020).

reached −12.25 m yr^{-1} (LRR). Area D displayed the most dramatic changes following 2015, with severe erosion (NSM = −855.09 m; LRR = −34.71 m yr^{-1}) alongside localized accretion of +256.81 m (NSM). In Area E, retreat dominated, with maximum NSM erosion of −989.86 m and an annual regression rate of −57.92 m yr^{-1} (LRR). Figs. 10 and 11 show NSM and Figs. 12 and 13 show LRR in the Ziarat estuary.

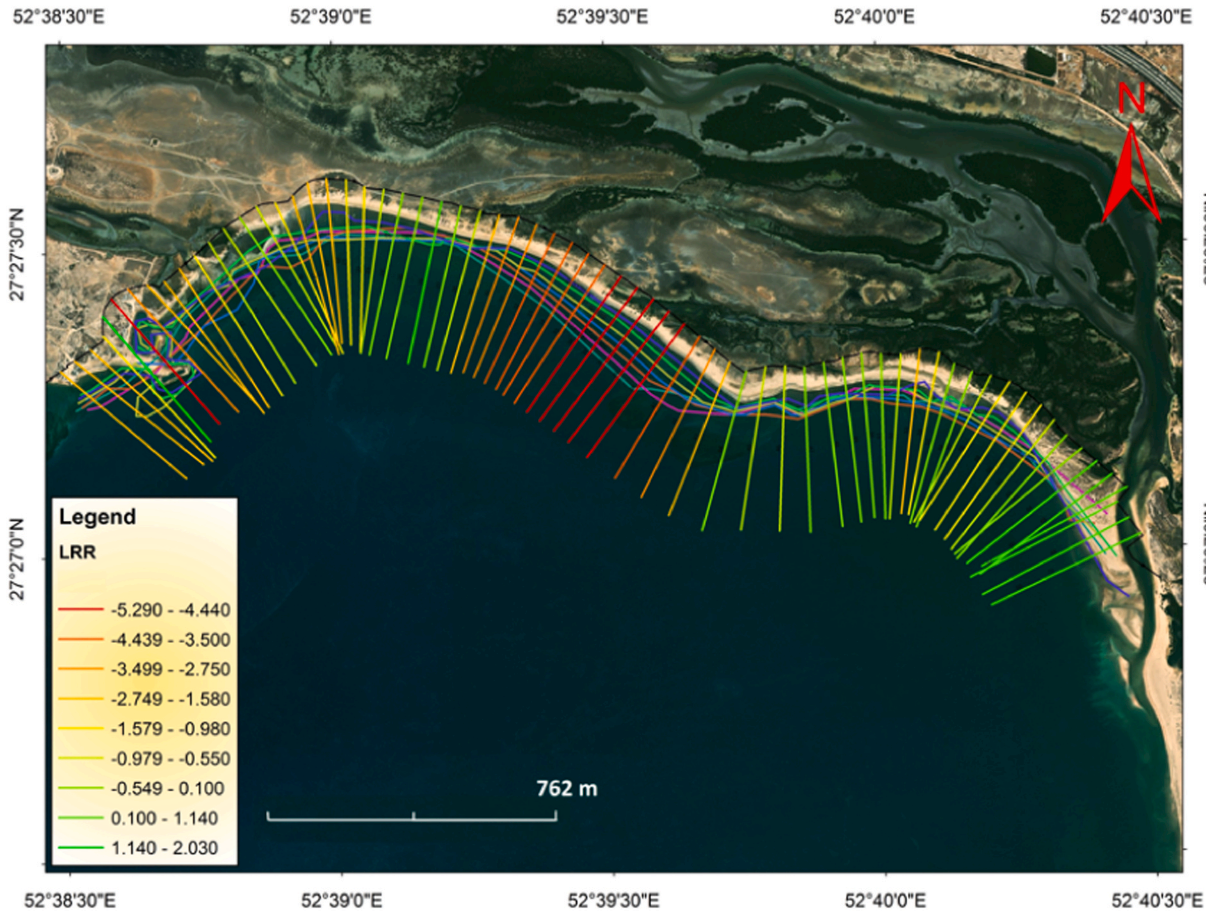

Fig. 7. Shoreline change rate (1990–2020) using the Linear regression rate (LRR) along the Bidkhoon estuary.

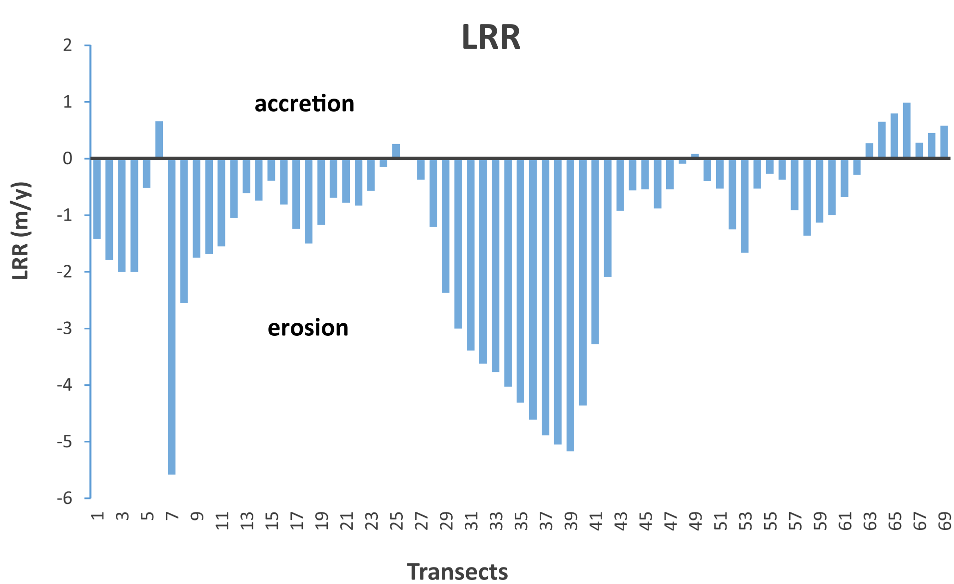

Fig. 8. Shoreline accretion and erosion rates using Linear regression rate (LRR) along the Bidkhoon estuary (1990–2020).

4.3. Shoreline dynamics in the Shif estuary

The Shif estuary, one of the region's most productive estuarine systems, exhibited the highest magnitude of shoreline variability (Fig. 14). High-tide Landsat imagery revealed distinct patterns across two primary sectors. In Area A, located within the protected Helleh region, alternating cycles of advancement and retreat occurred from 2000 to 2019. NSM recorded extreme erosion of −2022 m and an annual LRR rate of -57.67 m yr^{-1}. Area B, adjacent to aquaculture sites and facing Shif Island, exhibited comparatively subtle changes. Maximum NSM values indicated −166 m of retreat and +174.29 m of accretion, with LRR values varying from −24.88 to +11.26 m yr^{-1}. Overall, the Shif

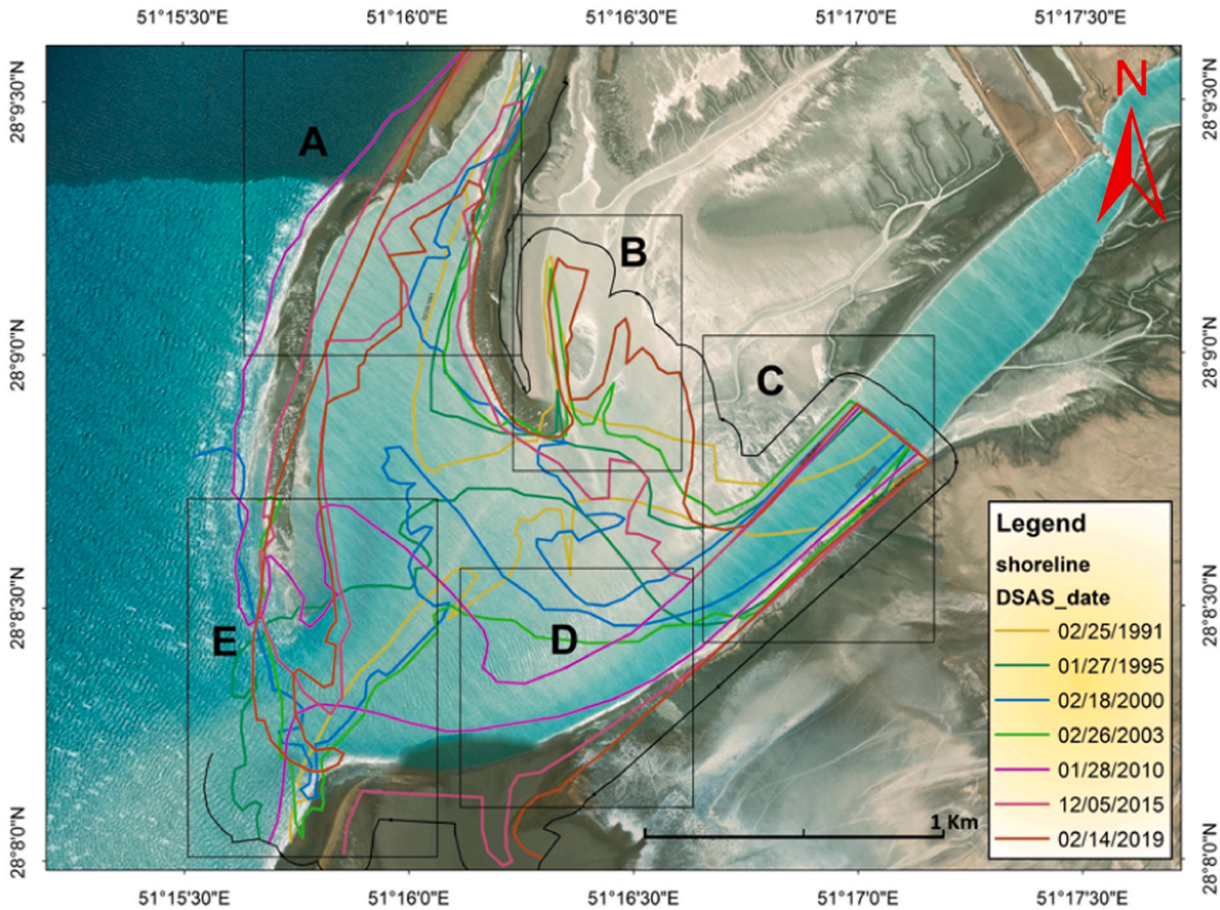

Fig. 9. Shoreline extraction using MNDWI on Landsat imagery along the Ziarat estuary (1990–2020). The line color show the date of shoreline extraction, This coastline was segmented into five (A,B,C,D,E) distinct zones.

estuary demonstrated a complex interplay between hydrodynamic forces and human modifications, resulting in both severe erosion and localized accretion. Figs. 15 and 16 show NSM and Figs. 17 and 18 show LRR in the Shif estuary.

Table 6 consolidates the mean, maximum erosion, and maximum accretion values for NSM and LRR across all three estuaries. The highest erosion (−2332 m) and accretion (+1326 m) values occurred in the Shif estuary, while Ziarat recorded the strongest net retreat rates (LRR = −57.92 m yr^{-1}). Bidkhoon remained the most morphologically stable system.

5. Discussion

Shoreline evolution in estuarine environments results from the complex interaction of marine hydrodynamics, sediment supply, river discharge, coastal geomorphology, and human activities (Mishra et al., 2026). Long-term monitoring of shoreline position is therefore essential for understanding coastal dynamics and supporting sustainable management, particularly in ecologically sensitive estuaries where relatively small shoreline displacements may substantially affect coastal habitats and ecosystem functions (Nassar et al., 2018; Guchhait et al., 2026). In the present study, multi-temporal Landsat imagery combined with MNDWI-based shoreline extraction and DSAS analysis was used to quantify shoreline changes in the three largest estuaries of Bushehr Province over approximately three decades. These three major estuaries located within or adjacent to protected coastal environments, including Nayband National Marine Park, the Mond Protected Area, and the Helle Protected Area. These environments support tidal wetlands, mangrove habitats, fisheries, migratory birds, and other coastal ecosystems that are highly sensitive to geomorphological changes. Furthermore, estuarine systems in arid regions generally receive limited freshwater inflow and sediment supply, making them particularly vulnerable to shoreline migration.

The Bidkhoon Estuary exhibited the lowest shoreline variability among the three investigated estuaries, indicating a comparatively stable estuarine system despite the predominance of shoreline retreat. Although erosion was the dominant process along most transects, localized shoreline accretion suggests that sediment redistribution remains active within the estuary, reflecting the dynamic equilibrium commonly observed in estuarine environments where erosion and deposition occur simultaneously under the influence of tidal currents, wave action, and local sediment transport processes. Compared with river-dominated estuaries, Bidkhun receives no permanent freshwater inflow, and its shoreline evolution is therefore likely controlled primarily by marine processes and local sediment redistribution rather than by substantial variations in fluvial sediment discharge. However, because hydrodynamic conditions and sediment transport were not directly measured in the present study, these factors should be regarded as plausible explanations rather than confirmed mechanisms. The observed shoreline behavior is consistent with previous investigations along the Asaluyeh–Nayband coastal sector, which similarly reported moderate but spatially variable shoreline changes controlled largely by local geomorphological conditions rather than by a uniform regional trend (Salami et al., 2014; Parhizkar et al., 2019). Comparable shoreline responses have also been documented in estuarine environments outside Iran, including the Atlantic coast of Morocco (Moussaid et al., 2015), the Gulf of Khambhat (Jodhani et al., 2024), and southeastern Australia (Konlechner et al., 2020), where shoreline evolution has likewise been

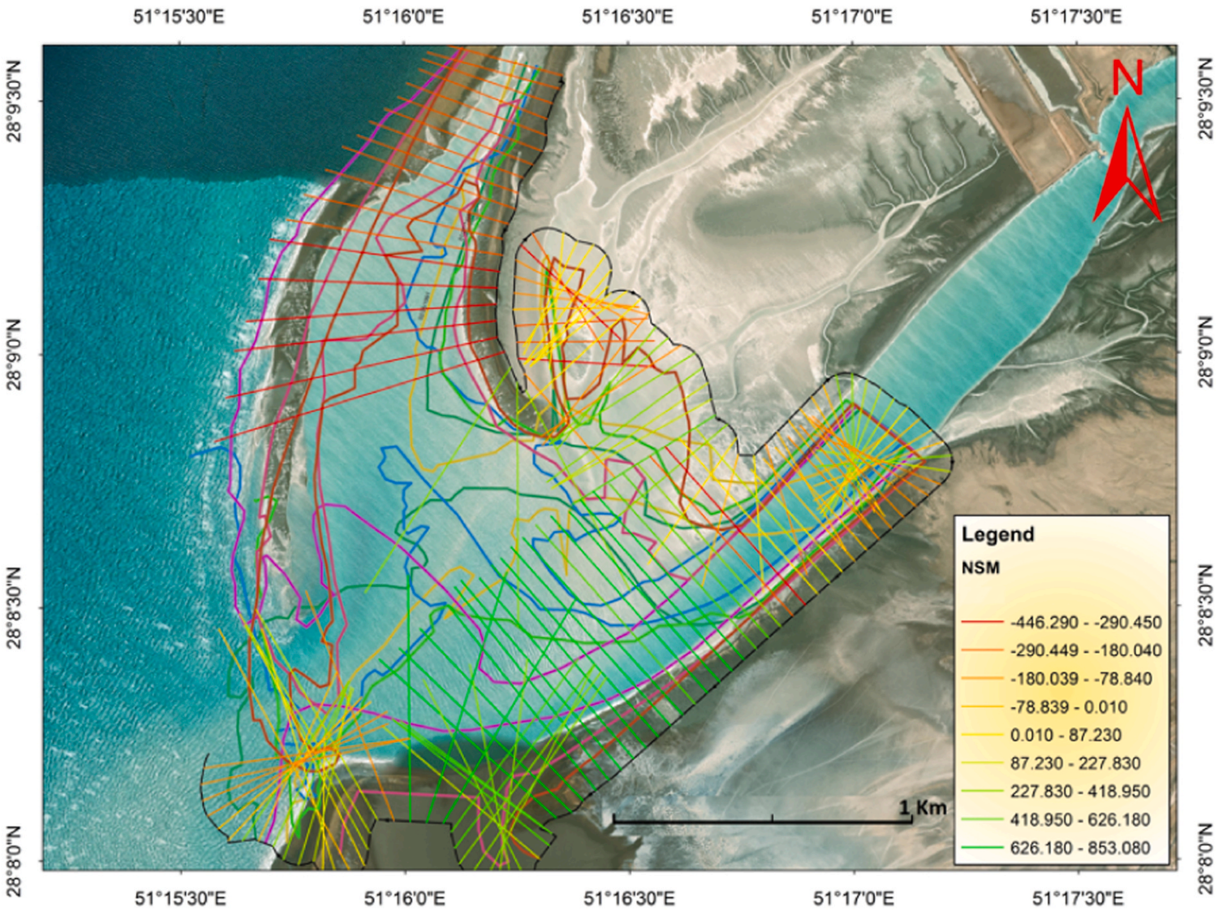

Fig. 10. Shoreline change (1990–2020) using the Net shoreline changes (NSM) (m) along the Ziarat estuary.

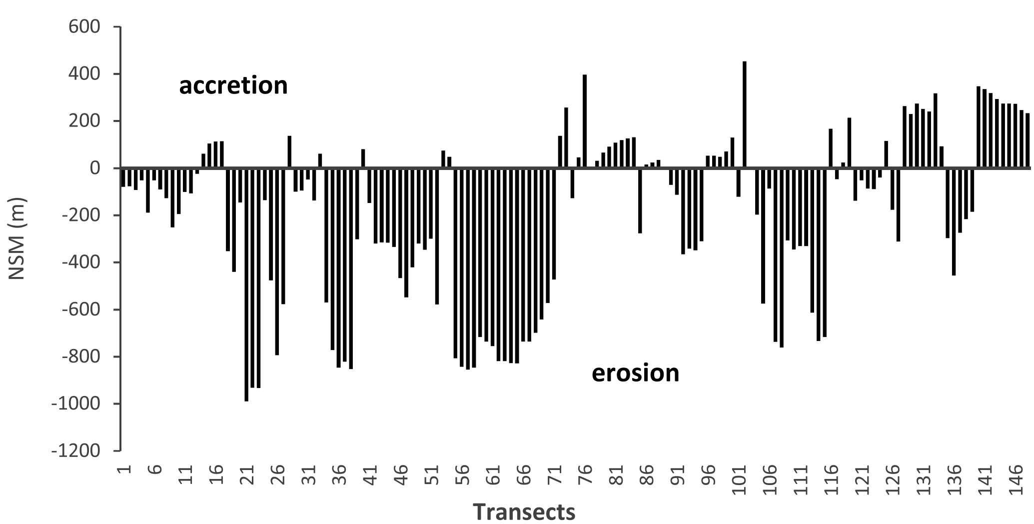

Fig. 11. Net shoreline changes (NSM) (m), shoreline accretion and erosion along the Ziarat estuary (1990–2020).

shown to depend strongly on estuarine morphology, sediment availability, and local hydrodynamic processes.

The Ziarat Estuary exhibited substantially greater shoreline retreat than the Bidkhun Estuary, indicating a more dynamic estuarine environment along the northern Persian Gulf. Located at the mouth of the Mond River, this estuary is continuously influenced by the interaction between fluvial and marine processes, resulting in pronounced spatial variability in erosion and accretion. Similar shoreline behavior has previously been reported for the Mond River delta, where multi-temporal Landsat analysis identified the estuary mouth as the most geomorphologically active sector of the coastline (Taghavi-Moghadam et al., 2018). Comparable patterns have also been documented in other estuarine environments, where shoreline evolution reflects local sediment budgets and estuarine morphology rather than a uniform regional response (Appeaning Addo et al., 2011; Moussaid et al., 2015). The mean shoreline retreat observed in the present study (LRR =

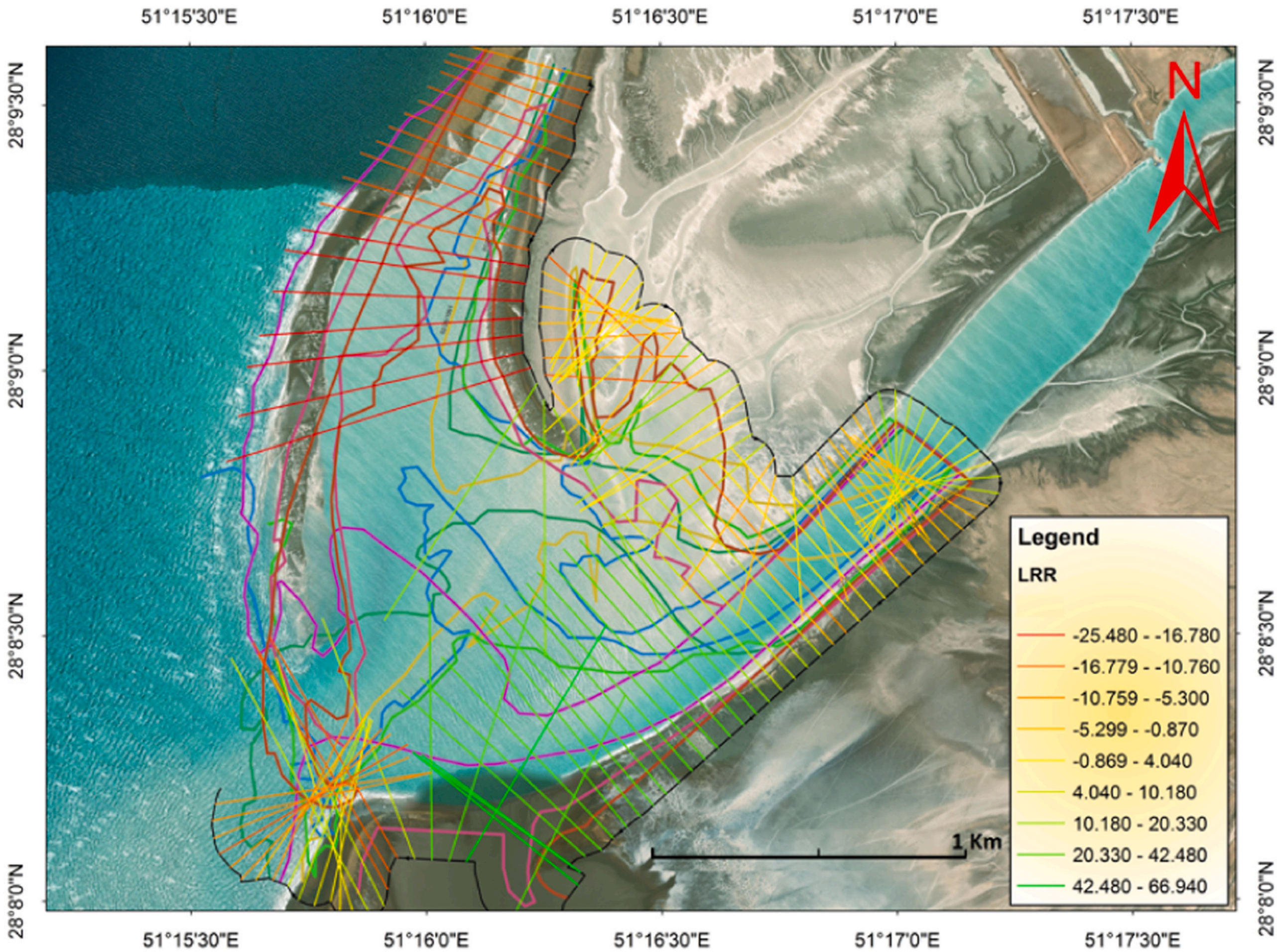

Fig. 12. Shoreline change rate (1990–2020) using the Linear regression rate (LRR) along the Ziarat estuary.

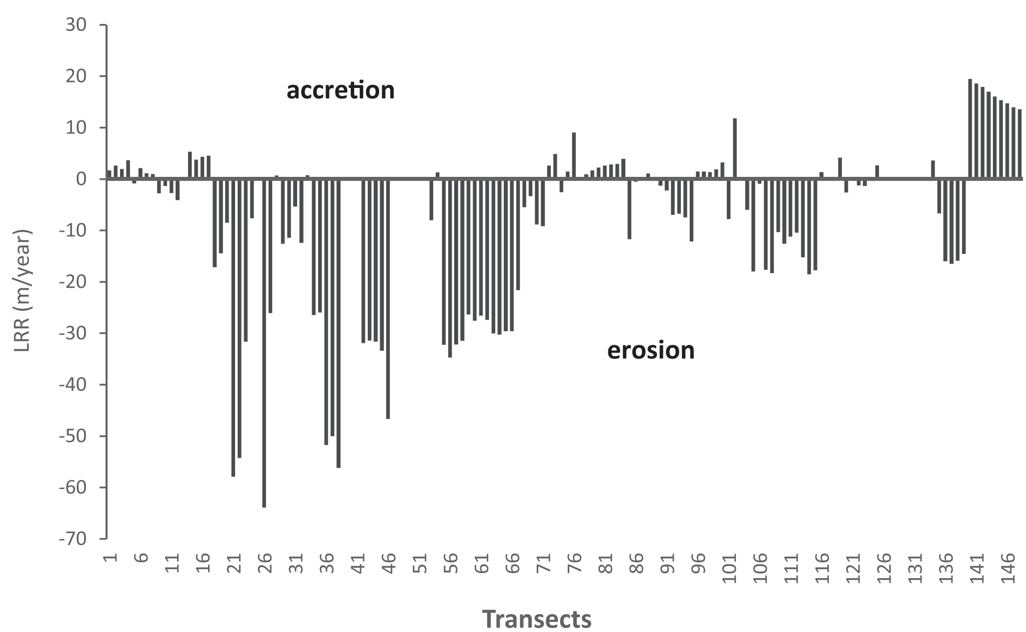

Fig. 13. Linear regression rate (LRR), shoreline accretion and erosion rates along the Ziarat estuary (1990–2020).

-9.02 m yr^{-1}) is also comparable with erosion rates reported for other sediment-limited estuarine and river-mouth environments worldwide, including approximately -10 m yr^{-1} along the southern Sulina mouth of the Danube River and about -18 m yr^{-1} at the Yeşilırmak River mouth

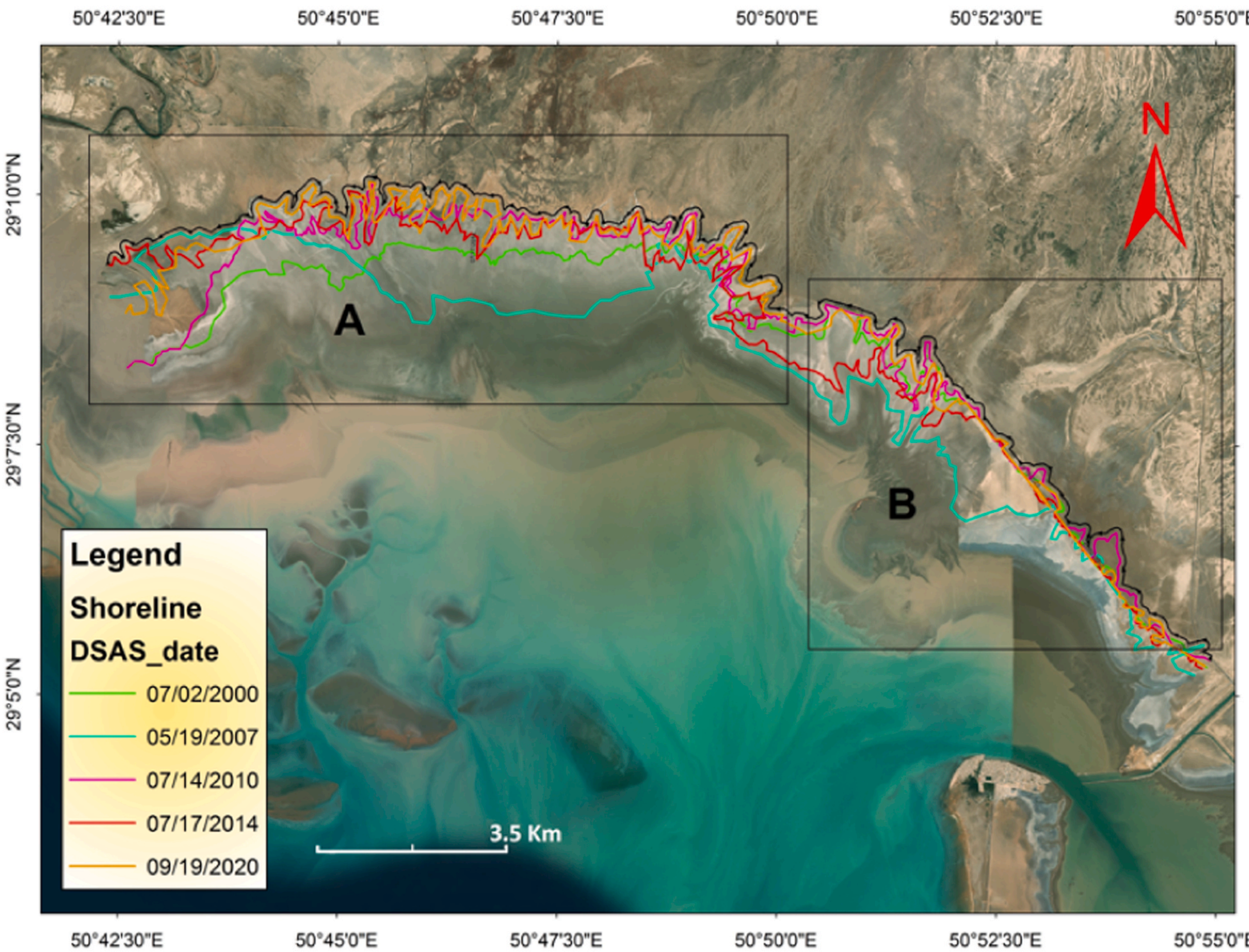

Fig. 14. Shoreline extraction using MNDWI on Landsat imagery along the Shif estuary (1990–2020) The line colors show the date of shoreline extraction, This coastline was segmented into two (A,B) distinct zones.

(Luijendijk et al., 2018). Likewise, Gormüs et al., (2021) reported shoreline retreat rates of approximately −18 m yr^{-1} for the Danube Delta and −22.6 m yr^{-1} for the Yeşilırmak Delta, demonstrating that river-mouth environments commonly experience rapid shoreline adjustment in response to variations in sediment supply and coastal hydrodynamics.

Several regional studies suggest that the observed shoreline retreat may be associated with changes in sediment supply and coastal hydrodynamics. Suspended sediment records from the Ghantareh hydrometric station indicate a declining trend in sediment discharge from the Mond River after 2001, attributed to upstream diversion dams and reduced regional precipitation (Ministry of Energy, 2011). Similar relationships between river regulation, sediment reduction, and shoreline retreat have been documented in many coastal environments. Ataol et al. (2019) concluded that river regulation was the principal factor controlling long-term shoreline changes in the Kızılırmak Delta, whereas Syvitski et al. (2009) and Snoussi et al. (2002) demonstrated that sediment trapping behind dams substantially reduces sediment delivery to downstream coasts. Likewise, Kermani et al. (2016) showed that dam construction on the El Kebir and Djen-Djen rivers significantly decreased sediment inputs to the Bay of Jijel, thereby intensifying coastal erosion.

In addition, hydrodynamic studies have shown that the interaction between tidal currents and prevailing wind-driven circulation controls sediment redistribution along the Mond delta (Naeimi et al., 2010). Relative sea-level rise along the northern Persian Gulf, estimated at approximately 4 mm yr^{-1} and potentially enhanced by regional subsidence (Etemadi et al., 2021), together with documented coastal inundation in the Mond delta (Taghavi Moghaddam, 2011), may further increase shoreline vulnerability. However, because sediment transport, subsidence, and sea-level change were not directly quantified in the present study, these factors are interpreted as plausible regional drivers supported by previous investigations rather than definitive causes of the observed shoreline retreat.

The Shif Estuary exhibited the greatest shoreline variability among the three investigated estuaries, as evidenced by the largest values of both erosion and accretion. Unlike the Bidkhun and Ziarat estuaries, where shoreline retreat predominated, the Shif Estuary displayed a complex spatial pattern characterized by localized erosion in some sectors and substantial shoreline advancement in others. This heterogeneous behavior suggests that shoreline evolution in the estuary is controlled by highly dynamic sediment redistribution rather than by a uniform erosional trend. Similar spatial variability has previously been reported for the Helleh estuarine system, where severe erosion occurred near the Helleh Gulf, whereas sediment accumulation was observed along the Shif and Bushehr coastlines (Salami et al., 2014), supporting the spatial patterns identified in the present study.

The contrasting shoreline responses observed in the Shif Estuary are likely related to the interaction of riverine sediment supply, tidal currents, and local anthropogenic activities. The Helleh River discharges freshwater and sediment into the estuary, providing an important sediment source that may promote localized accretion under favorable hydrodynamic conditions. In addition, aquaculture facilities established along parts of the estuary may modify local flow patterns and enhance sediment trapping, thereby contributing to shoreline advancement in

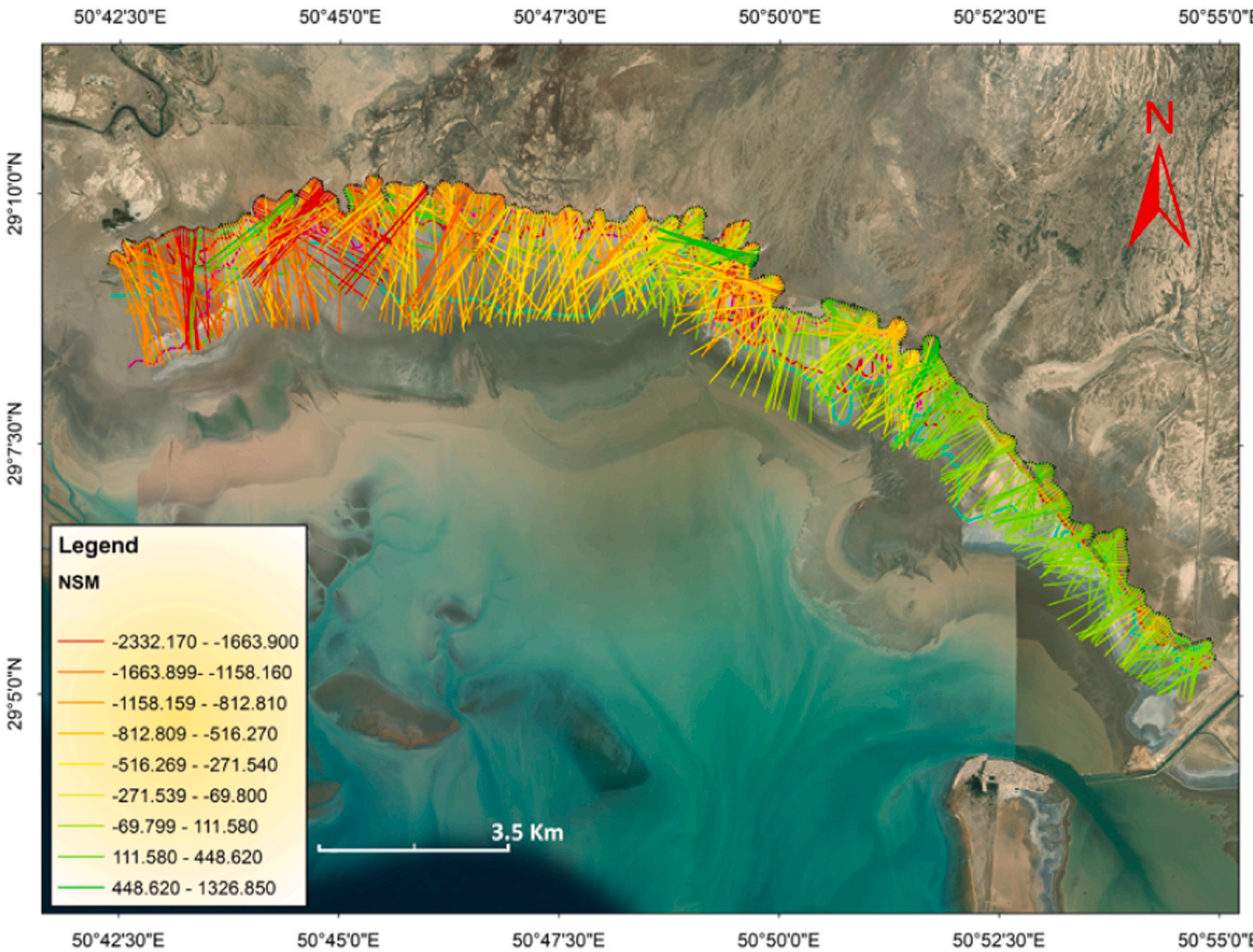

Fig. 15. Shoreline change (1990–2020) using the Net shoreline changes (NSM) (m) along the Shif estuary.

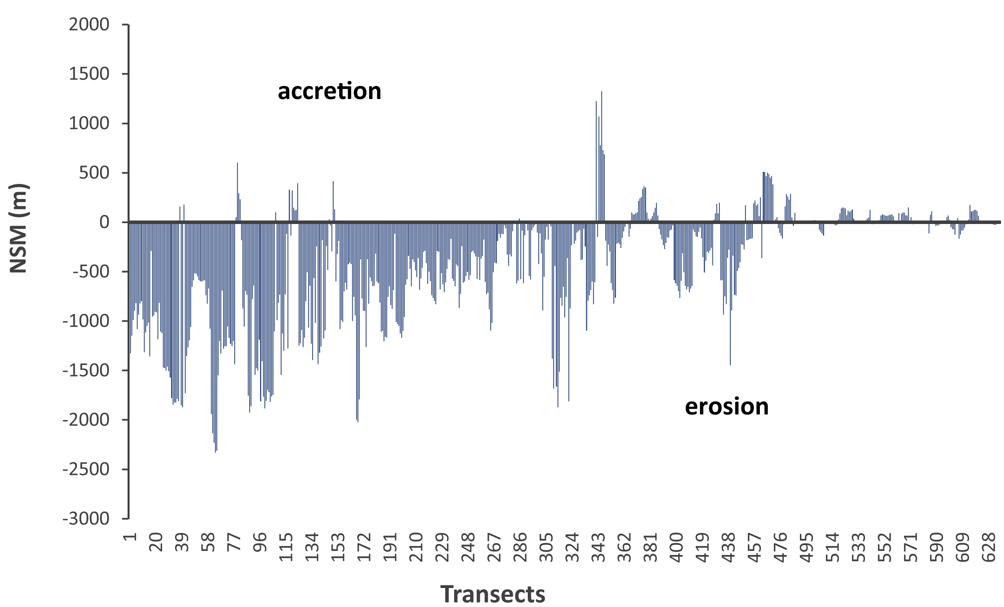

Fig. 16. Net shoreline changes (NSM) (m), shoreline accretion and erosion along the Shif estuary (1990–2020).

sheltered areas. However, these structures may also alter sediment redistribution pathways and increase erosion elsewhere along the shoreline. Similar effects of coastal infrastructure on sediment transport and shoreline evolution have been reported in other estuarine environments (Dugan et al., 2011; Jiang et al., 2024). Nevertheless, because hydrodynamic processes and sediment transport were not directly

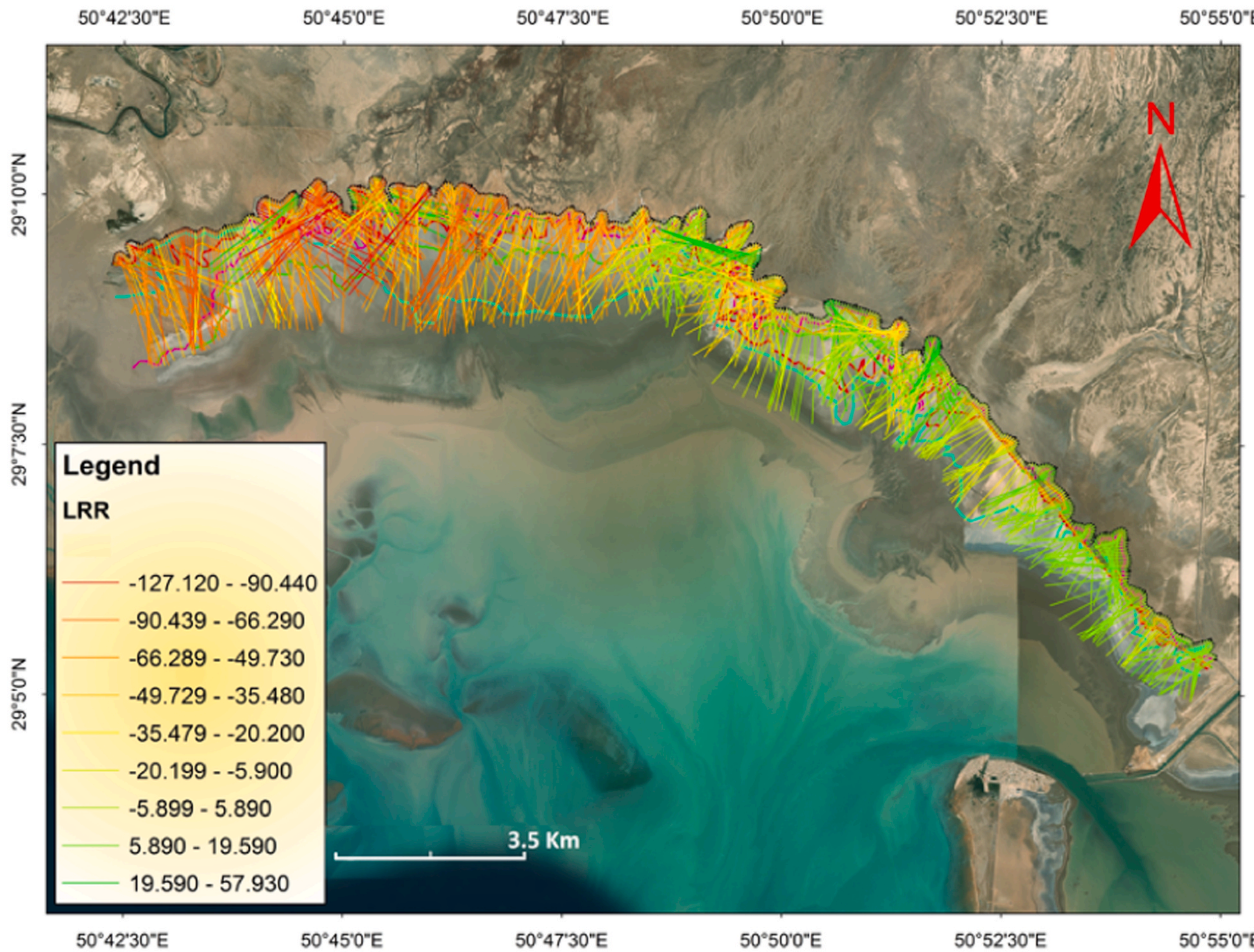

Fig. 17. Shoreline change rate (1990–2020) using the Linear regression rate (LRR) along the Shif estuary.

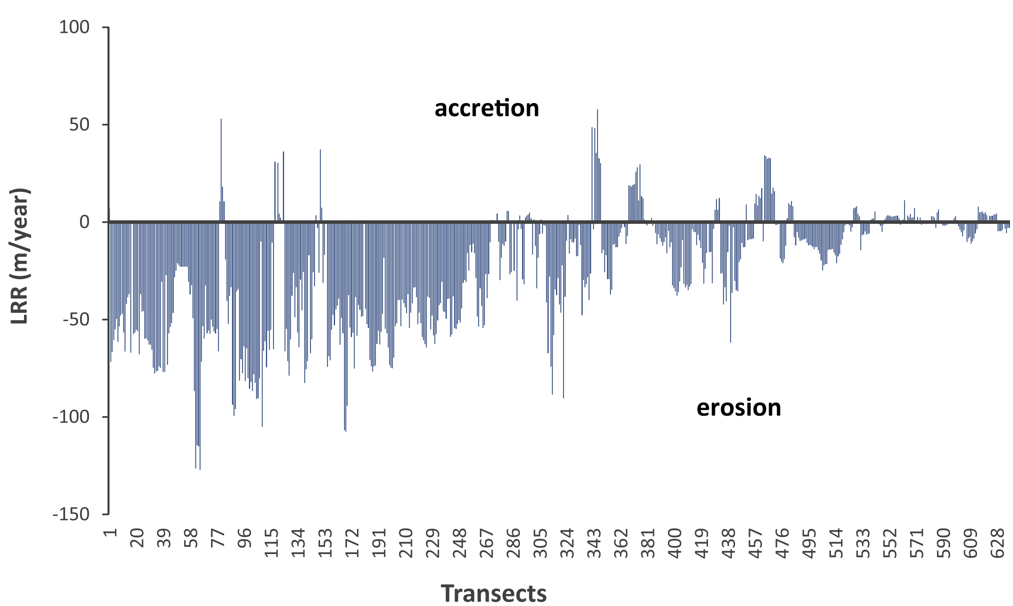

Fig. 18. Linear regression rate (LRR), shoreline accretion and erosion rates along the Shif estuary (1990–2020).

measured in this study, these factors should be considered plausible mechanisms rather than definitive causes of the observed shoreline changes.

The shoreline dynamics identified in the Shif Estuary are also consistent with observations from comparable estuarine environments worldwide. For example, Khanmohamadi et al., (2019) reported the

Table 6
Statistical parameters obtained from DSAS analysis in the study area (1991–2022) in Bidkhoon, Ziarat, and Shif estuaries in the 1990–2020 period.

Study area	Index	Max accretion	Min accretion	Mean (m/y) ±SD	Max erosion	Min erosion	Total length of accreted shoreline(m)	Total length of eroded shoreline(m)	Number of trancects
Bidkhoon	NSM	97.88	5.33	−34.34 ± 42	−147.65	−3.83	275(14%)	1725 (85%)	69
	LRR	2.03	0.26	−1.41 ± 1.2	−5.29	−0.15			
Ziarat	NSM	452.05	14.9	−210.64 ± 290	−989.86	−25.14	2760(31%)	6000 (67%)	146
	LRR	19.49	0.43	−9.02 ± 13	−63.91	−0.82			
Shif	NSM	1326.85	21.2	−431.23 ± 560	−2332.17	−20.8	7800(20%)	29880(78%)	628
	LRR	57.93	1.2	−25.20 ± 36	−127.12	−1.1			

coexistence of erosion and extensive shoreline progradation along the Iranian coast of the Oman Sea, demonstrating the importance of spatially variable sediment transport in shaping coastal morphology. Likewise, Salauddin et al. (2018) documented simultaneous landward retreat (−2680 m) and seaward advancement (+1897 m) at the Meghna River estuary in Bangladesh, highlighting that estuarine environments commonly exhibit alternating erosion and accretion owing to continuous sediment redistribution. These similarities indicate that the complex shoreline behavior observed in the Shif Estuary represents a characteristic response of sediment-rich estuarine systems rather than an isolated regional phenomenon. Similar spatially heterogeneous shoreline responses have been reported for estuarine systems in different parts of the world, including the Mediterranean coast, the Bay of Bengal, the Black Sea, and southeastern Australia, where long-term shoreline evolution has been shown to vary substantially even between neighboring estuaries because of differences in sediment budgets, tidal regimes, and coastal morphology (Mukhopadhyay et al., 2012; Moussaid et al., 2015; Konlechner et al., 2020; Gormüs et al., 2021).

The comparison of the three estuaries demonstrates that shoreline evolution along the northern Persian Gulf is highly site-specific, even within a relatively limited geographical region. Bidkhun exhibited comparatively stable shoreline behavior, reflecting the dominance of marine processes under limited fluvial sediment input. In contrast, the Ziarat Estuary experienced the greatest erosion, highlighting the sensitivity of river-mouth environments to variations in sediment supply and coastal hydrodynamics. The Shif Estuary displayed the highest spatial variability, characterized by the coexistence of erosion and accretion, indicating that sediment redistribution processes remain highly active within this estuarine system.

Despite these contributions, several limitations should be acknowledged. Although shoreline extraction uncertainty associated with image registration, digitization, tidal stage, and sensor characteristics was minimized through geometric correction, the use of stable ground control points, comparable High Water Level (HWL) conditions, and consistent Landsat spatial resolution, the study did not directly quantify sediment transport, hydrodynamic processes, subsidence, or relative sea-level rise. Consequently, these factors were interpreted using supporting regional studies rather than direct field measurements. Future investigations integrating remote sensing with hydrodynamic modeling, sediment budget analyses, continuous GPS observations, and higher-resolution satellite or UAV imagery would improve the understanding of the physical mechanisms controlling shoreline evolution in the northern Persian Gulf.

6. Conclusion

Multi-temporal Landsat imagery combined with the Digital Shoreline Analysis System (DSAS) successfully characterized three decades of shoreline evolution in the Bidkhhoon, Ziarat, and Shif estuaries along the northern Persian Gulf. The results demonstrate that shoreline behavior differs markedly among neighboring estuaries, indicating that coastal evolution is governed by local environmental conditions rather than by a uniform regional trend.

Among the investigated estuaries, Ziarat experienced the most persistent shoreline retreat, whereas Bidkhhoon showed moderate erosion and Shif exhibited the greatest spatial variability, with erosion and accretion occurring simultaneously in different sectors. These contrasting patterns emphasize the dynamic nature of estuarine coastlines and the importance of evaluating shoreline changes at the local scale.

The observed shoreline changes are consistent with regional evidence of variations in sediment supply and coastal hydrodynamics, although the relative contribution of individual processes could not be quantified within the scope of this study. Consequently, further investigations integrating hydrodynamic modelling, sediment transport measurements, and higher-resolution observations are required to better understand the mechanisms controlling shoreline evolution.

Overall, the findings provide an updated understanding of long-term shoreline dynamics in the northern Persian Gulf and establish a reference dataset for future coastal monitoring and environmental management of these estuarine systems.

CRediT authorship contribution statement

Hamid Amoonia: Investigation, Formal analysis. **Esmaeil Abbasi:** Investigation, Formal analysis, Data curation. **Hana Etemadi:** Writing – original draft, Validation, Supervision, Software, Resources, Methodology, Investigation, Formal analysis, Data curation, Conceptualization. **Shiva Rastgou:** Investigation, Formal analysis, Data curation.

Funding

There is no funding sources in this research.

Declaration of Competing Interest

The authors declare that they have no known competing financial interests or personal relationships that could have appeared to influence the work reported in this paper.

Data availability

Data will be made available on request.

References

Abbasi, E., Etemadi, H., Krzyszczak, J., 2024. Habitat suitability and flood risk modeling for Gazella conservation actions in Mond protected area. Int. J. Disaster Risk Reduct. 113, 104816. https://doi.org/10.1016/j.ijdrr.2024.104816.

Abbasi, E., Etemadi, H., Smoak, J.M., Rousta, I., Olafsson, H., Baranowski, P., Krzyszczak, J., 2021. Investigation of atmospheric conditions associated with a storm surge in the south-west of Iran. Atmosphere 12 (11), 1429. https://doi.org/10.3390/atmos12111429.

Alesheikh, A.A., Ghorbanali, A., Nouri, N., 2007. Coastline change detection using remote sensing. Int. J. Environ. Sci. Technol. 4 (1), 61–66. https://doi.org/10.1007/BF03325962.

Appeaning Addo, K.A., Jayson-Quashigah, P.N., Kufogbe, K.S., 2011. Quantitative analysis of shoreline change using medium resolution satellite imagery in Keta, Ghana. Mar. Sci. 1 (1), 1–9. https://doi.org/10.5923/j.ms.20110101.01.

Appeaning Addo, K.A., Walkden, M., Mills, J., 2008. Detection, measurement and prediction of shoreline recession in Accra, Ghana. ISPRS J. Photogramm. Remote. Sens. 63, 543–558. https://doi.org/10.1016/j.isprsjprs.2008.04.001.

Ataol, M., Kale, M.M., Tekkanat, I.S., 2019. Assessment of the changes in shoreline using digital shoreline analysis system: a case study of Kızılırmak Delta in northern Turkey from 1951 to 2017. Environ. Earth Sci. 78, 579. https://doi.org/10.1007/s12665-019-8591-7.

Ayadi, K., Boutiba, M., Sabatier, F., Guettouche, M.S., 2016. Detection and analysis of historical variations in the shoreline, using digital aerial photos, satellite images, and topographic surveys DGPS: Case of the Bejaia bay (East Algeria). Arab. J. Geosci. 9 (1), 26. https://doi.org/10.1007/s12517-015-2043-9.

Bera, R., Maiti, R., 2019. Quantitative analysis of erosion and accretion (1975-2017) using DSAS-A study on Indian Sundarbans. Reg. Stud. Mar. Sci. 28, 100583. https://doi.org/10.1016/j.rsma.2019.100583.

Boak, E.H., Turner, I.L., 2005. Shoreline definition and detection: A review. J. Coast. Res. 21 (4), 688–703. https://doi.org/10.2112/03-0071.1.

Crain, C.M., Halpern, B.S., Beck, M.W., Kappel, C.V., 2009. Understanding and managing human threats to the coastal marine environment. Ann. N. Y. Acad. Sci. 1162, 39–62. https://doi.org/10.1111/j.1749-6632.2009.04496.x.

Crowell, M., Leatherman, S.P., Buckley, M.K., 1991. Historical shoreline change: error analysis and mapping accuracy. J. Coast. Res. 7, 839–852.

Das, A., Mondal, I., Hossain, S.K.A., Jose, A., Ouda, M., Juliev, M., Almaliki, A.H., Kumar De, T., 2025. Coastal vulnerability assessment for the Sundarbans mangrove ecosystem using InVEST and machine learning based empirical models. Environ. Dev. Sustain. https://doi.org/10.1007/s10668-025-06414-x.

Davidson, M.A., Lewis, R.P., Turner, I.L., 2010. Forecasting seasonal to multi-year shoreline change. Coast. Eng. 57, 620–629. https://doi.org/10.1016/j.coastaleng.2010.02.001.

Del Río, L., Gracia, F.J., 2012. Error determination in the photogrammetric assessment of shoreline changes. Nat. Hazards. https://doi.org/10.1007/s11069-012-0407-y.

Dugan, J.E., Airoldi, L., Chapman, M.G., Walker, S.J., Schlacher, T., 2011. Estuarine and coastal structures: environmental effects, a focus on shore and nearshore structures. In E. Wolanski & D. McLusky (Eds.), Treatise on estuarine and coastal science. (Vol. 8, pp. 17-41). https://doi.org/10.1016/B978-0-12-374711-2.00802-0.

Etemadi, H., Samadi, S.Z., Sharifikia, M., Smoak, J.M., 2016. Assessment of climate change downscaling and non-stationarity on the spatial pattern of a mangrove ecosystem in an arid coastal region of southern Iran. Theor. Appl. Climatol. 126 (1-2), 35–49. https://doi.org/10.1007/s00704-015-1552-5.

Etemadi, H., Smoak, J.M., Abbasi, E., 2021. Spatiotemporal pattern of degradation in arid mangrove forests of the Northern Persian Gulf. Oceanologia 63 (1), 99–114. https://doi.org/10.1016/j.oceano.2020.10.003.

Etemadi, H., Smoak, J.M., Karami, J., 2018. Land use change assessment in coastal mangrove forests of Iran utilizing satellite imagery and CA-Markov algorithms to monitor and predict future change. Environ. Earth Sci. 77 (5), 208. https://doi.org/10.1007/s12665-018-7392-8.

Gopinath, G., Thodi, M.F.C., Surendran, U.P., Prem, P., Parambil, J.N., Alataway, A., Al-Othman, A.A., Dewidar, A.Z., Mattar, M.A., 2023. Long-term shoreline and islands change detection with digital shoreline analysis using RS data and GIS. Water 15, 244. https://doi.org/10.3390/w15020244.

Gormüs, T., Ayat, B., Aydogan, B., Tatui, F., 2021. Basin scale spatiotemporal analysis of shoreline change in the Black Sea. Estuar. Coast. Shelf Sci. 252, 107247. https://doi.org/10.1016/j.ecss.2021.107247.

Guchhait, S., Mishra, M., Goswami, S., Paul, S., Guria, R., da, Silva, R.M., Islam, A.R.M. T., 2026. Charting the future of coastal resilience: A three-decade global exploration of coastal vulnerability science and strategic gaps. Reg. Stud. Mar. Sci., 104875 https://doi.org/10.1016/j.rsma.2026.104875.

Gunasegaram, P., Kankara, R.S., Selvan, S.C., 2022. Mapping shoreline changes of the pocket beaches using remote sensing and GIS – a study in the north Konkan sector, west coast of India. J. Earth Syst. Sci. 131 (209), 1–15. https://doi.org/10.1007/s12040-022-01945-7.

Hakko, M., Maanan, M., Belrhaba, T., El khalidi, K., El Ouai, D., Benmohammadi, A., 2018. Multi-decadal assessment of shoreline changes using geospatial tools and automatic computation in Kenitra coast, Morocco. Ocean. Coast. Manag. 163, 232–239. https://doi.org/10.1016/j.ocecoaman.2018.07.003.

Hapke, C.J., Himmelstoss, E.A., Kratzmann, M., List, J.H., & Thieler, E.R. (2010). *National assessment of shoreline change: Historical shoreline change along the New England and Mid-Atlantic coasts* (US Geological Survey Open-File Report 1118, p. 57).

Harley, C.D.G., Hughes, A.R., Hultgren, K.M., Miner, B.G., Sorte, C.J.B., Thornber, C.S., Rodriguez, L.F., Tomanek, L., Williams, S.L., 2006. The impacts of climate change in coastal marine systems. Ecol. Lett. 9, 228–241. https://doi.org/10.1111/j.1461-0248.2005.00871.x.

Hecht, C.W., Cordeira, J.M., 2017. Characterizing the influence of atmospheric river orientation and intensity on precipitation distributions over North Coastal California. Geophys. Res. Lett. 44, 9048–9058. https://doi.org/10.1002/2017GL074179.

Hossain, S.K., Mondal, I., Thakur, S., Fadhil Al-Quraishi, A.M., 2022a. Coastal vulnerability assessment of India's Purba Medinipur-Balasore coastal stretch: a comparative study using empirical models. Int. J. Disaster Risk Reduct. 77, 103065. https://doi.org/10.1016/j.ijdrr.2022.103065.

Hossain, S.A., Mondal, I., Thakur, S., Linh, N.T.H., Anh, D.T., 2022b. Assessing the multidecadal shoreline dynamics along the Purba Medinipur-Balasore coastal stretch, India by integrating remote sensing and statistical methods. Acta Geophys. https://doi.org/10.1007/s11600-022-00797-5.

Jiang, J., Xie, W., Zhang, N., Xu, Y., Zhu, C., Lin, J., Guo, L., Shen, J., He, Q., 2024. Mechanism of rapid accretion-erosion transition in a complex hydrodynamic environment based on refined in-situ data. Front. Mar. Sci. 11, 1375085. https://doi.org/10.3389/fmars.2024.1375085.

Jodhani, K., Bansal, P., Jain, P., 2021. Shoreline Change and Rate Analysis of Gulf of Khambhat Using Satellite Images. In: Mehta, Y.A., Carnacina, I., Kumar, D.N., Rao, K.R., Kumari, M. (Eds.), Advances in Water Resources and Transportation Engineering. Lecture Notes in Civil Engineering, 149. Springer, Singapore. https://doi.org/10.1007/978-981-16-1303-6_12.

Jodhani, K.H., Patel, D., Madhavan, N., 2024. Identification of Sensitive Region by Short Term Shoreline Change Analysis Over Gulf of Khambhat, Gujarat. In: Mudgal, A., Davies, P., Kennedy, M., Zaragoza, G., Park, K. (Eds.), Advances in Water Treatment and Management. ICAWTM 2023. Lecture Notes in Civil Engineering, 536. Springer, Singapore. https://doi.org/10.1007/978-981-97-5955-2_7.

Jonah, F.E., Boateng, I., Osman, A., Shimba, M.J., Mensah, E.A., Adu-Boahen, K., Effah, E., 2016. Shoreline change analysis using end point rate and net shoreline movement statistics: An application to Elmina, Cape coast and moore section of Ghana's coast. Reg. Stud. Mar. Sci. 7, 19–31. https://doi.org/10.1016/J.RSMA.2016.05.003.

Kermani, S., Boutiba, M., Guendouz, M., Guettouche, M.S., Khelfani, D., 2016. Detection and analysis of shoreline changes using geospatial tools and automatic computation: Case of Jillian sandy coast (East Algeria). Ocean. Coast. Manag. 132, 46–58. https://doi.org/10.1016/j.ocecoaman.2016.08.010.

Khanmohamadi, Z., Gharelou, S., Mahjobi, A., 2019. Investigation of periodic changes in the coastline of the Sea of Oman using remote sensing data and spatial analysis. J. Environ. Eros. Res. 39 (3), 10.

Konlechner, T.M., Kennedy, D.M., O'Grady, J.J., Leach, C., Ranasinghe, R., Carvalho, R. C., Luijendijk, A.P., McInnes, K.L., Ierodiaconou, D., 2020. Mapping spatial variability in shoreline change hotspots from satellite data; a case study in southeast Australia. Estuar. Coast. Shelf Sci. 246, 107018. https://doi.org/10.1016/j.ecss.2020.107018.

Luijendijk, A., Hagenaars, G., Ranasinghe, R., Baart, F., Donchyts, G., Aarninkhof, S., 2018. The state of the world's beaches. Sci. Rep. 8, 6641. https://doi.org/10.1038/s41598-018-24630-6.

Martínez, M.L., Intralawan, A., Vázquez, G., Pérez-Maqueo, O., Sutton, P., Landgrave, R., 2007. The coasts of our world: ecological, economic and social importance. Ecol. Econ. 63, 254–272. https://doi.org/10.1016/j.ecolecon.2006.10.022.

Melet, A., Teatini, P., Le Cozannet, G., et al., 2020. Earth observations for monitoring marine coastal hazards and their drivers. Surv. Geophys. 41, 1489–1534. https://doi.org/10.1007/s10712-020-09594-5.

Miller, J.K., Dean, R.G., 2004. A simple new shoreline change model. Coast. Eng. 51, 531–556. https://doi.org/10.1016/j.coastaleng.2004.05.006.

Mills, J.P., Buckley, S.J., Mitchell, H.L., Clarke, P.J., Edwards, S.J., 2005. A geomatics data integration technique for coastal change monitoring. Earth Surf. Process. Landf. 30, 651–664. https://doi.org/10.1016/j.coastaleng.2004.05.006.

Ministry of Energy. (2011). *Delta research morphology* (No. 362 Technical Office). Tehran.

Mishra, M., Pati, S., Paul, S., Gonçalves, R.M., Acharyya, T., Tripathy, B., da, Silva, R.M., Guria, R., Santos, C.A.G., 2024b. Dynamic shoreline alterations and their impacts on Olive Ridley Turtle (*Lepidochelys olivacea*) nesting sites in Gahirmatha Marine Wildlife Sanctuary, Odisha (India). Mar. Pollut. Bull. 202, 116321. https://doi.org/10.1016/j.marpolbul.2024.116321.

Mishra, M., Zerouali, B., Paul, S., Bhattacharyya, D., Guria, R., Suna, M., Santos, C.A.G., 2026. Coastal futures at risk: Adaptive coastal management and policy insights from sea-level rise and shoreline change in West Bengal, India. Sci. Total. Environ. 1014, 181238. https://doi.org/10.1016/j.scitotenv.2025.181238.

Mondal, I., Bandyopadhyay, J., Dhara, S., 2017. Detecting shoreline changing trends using principle component analysis in Sagar Island, West Bengal, India. J. Spat. Inf. Res. 25 (1), 67–73. https://doi.org/10.1007/s41324-016-0076-0.

Mondal, I., Mishra, V., Hossain, S.K.A., Altuwaijri, H.A., Juliev, M., De, A., 2025. Mitigating coastal flood risks in the Sundarbans: A combined InVEST and machine learning approach. Phys. Chem. Earth 138, 103855. https://doi.org/10.1016/j.pce.2025.103855.

Mondal, I., Thakur, S., Juliev, M., Bandyopadhyay, J.D., 2020. Spatiotemporal modelling of shoreline migration in Sagar Island, West Bengal, India. J. Coast. Conserv. 24 (50), 1–20. https://doi.org/10.1007/s11852-020-00768-2.

Moore, L.J., 2000. Shoreline mapping techniques. J. Coast. Res. 16, 111–124.

Moussaid, J., Fora, A.A., Zourarah, B., Maanan, M., Maanan, M., 2015. Using automatic computation to analyze the rate of shoreline change on the Kenitra coast, Morocco. Ocean. Eng. 102, 71–77. https://doi.org/10.1016/j.oceaneng.2015.04.044.

Mukhopadhyay, A., Ghosh, P., Chanda, A., Ghosh, A., Ghosh, S., Das, S., Ghosh, T., Hazra, S., 2018. Threats to coastal community of Mahanadi delta due to imminent consequences of erosion – Present and near future. Sci. Total. Environ. 637–638, 717–729. https://doi.org/10.1016/j.scitotenv.2018.05.076.

Mukhopadhyay, A., Mukherjee, S., Mukherjee, S., Ghosh, S., Hazra, S., Mitra, D., 2012. Automatic shoreline detection and future prediction: A case study on Puri Coast, Bay of Bengal, India. Eur. J. Remote. Sens. 45, 201–213. https://doi.org/10.5721/EuJRS20124519.

Naeimi, N.A., Ghahroudi, T.M., Sarvati, M., 2010. Monitoring of coastal line and coastal landform changes in Persian Gulf with Remote Sensing and Geographic Information System Techniques (Case Study: Asaluyeh Coastal Region). Geogr. Space 10 (30), 45–61 (in Persian).

Nassar, K., Mohmod, W.E., Fath, H., Masria, A., Nadaoka, K., Negm, A., 2018. Shoreline change detection using DSAS technique: Case of North Sinai coast, Egypt. Mar. Georesour. Geotechnol. 37 (1), 81–95. https://doi.org/10.1080/1064119X.2018.1448912.

Parhizkar, F., Rajabi, M., Yamani, M., Mokhtari, D., 2019. Time variations analysis of the Hormoz strait northern shoreline by using Digital Shoreline Analysis System (DSAS).

J. Environ. Eros. Res. 9 (2), 1–18. http://magazine.hormozgan.ac.ir/article-1-509-fa.html.

Paul, S., Mishra, M., Guria, R., da, Silva, R.M., Santos, C.A.G., 2025. Geospatial analysis of shoreline dynamics and drivers in the sundarbans biosphere reserve (1990–2020): integrating natural and anthropogenic influences for coastal resilience. Sci. Total. Environ. 1001, 180494. https://doi.org/10.1016/j.scitotenv.2025.180494.

Razmi, M., Asgari, M.H., Dadolahi-Sohrab, A., Nazemossadat, S.M.J., Khazaei, S.H., 2018. Assessing changes shoreline in Dayyer city using the Landsat satellite data, sensor TM and OLI 1991 and 2014 years. J. Mar. Sci. Technol. 16, 1–12. https://doi.org/10.22113/jmst.2016.32078.

Salami, F., Azemode-Ardalan, A., Najafi-Alamdari, M., 2014. Monitoring coastal line changes using nautical charts in the management of coastal areas (Study area: Bushehr province). 20th Conferences of Geomatics. Tehran.

Salauddin, M., Tanim, A.H., Mehedi, I., 2018. Modeling spatio-temporal shoreline shifting of a coastal island in Bangladesh using geospatial techniques and DSAS extension. J. Geo-Environ. 18 (1), 1–13. https://doi.org/10.2478/AVUTGS-2018-0001.

Salehipour Milani, A., Eskansari, M., 2021. Monitoring and assessment of shorelines change in Makran geomorphological unit (Chabahar to Quatre). Q. J. Environ. Eros. Res. 43 (11), 1–26.

Snoussi, M., Haïda, S., Imassi, S., 2002. Effects of the construction of dams on the water and sediment fluxes of the Moulouya and the Sebou Rivers, Morocco. J. Mater. Cycles Waste Manag. 3 (1–3), 5–12. https://doi.org/10.1007/s10113-001-0035-7.

Sotoudepour, A., Madadi, A., Asghari Sareskanrood, S., 2020. Geomorphological monitoring of Bushehr port coastline, Iran. J. Geogr. Sci. 35 (2), 177–187.

Syvitski, J.P.M., Kettner, A.J., Overeem, I., Hutton, E.W.H., Hannon, M.T., Brakenridge, G.R., Day, J., Vörösmarty, C., Saito, Y., Giosan, L., Nicholls, R.J., 2009. Sinking deltas due to human activities. Nat. Geosci. 2, 681–686. https://doi.org/10.1038/ngeo629.

Taghavi Moghaddam, E., 2011. *Geomorphological developments of the north coast of the Persian Gulf from Bushehr to Kangan* [M.Sc. Thesis, Faculty of Geography. Kharazmi University, Tehran (in Persian).

Taghavi-Moghadam, A., Ghanavati, A., Akbari, A., Hoseini, H., 2018. Analysis of the geomorphodynamic changes in the coastline of the Mond Delta base in Bushehr using remote sensing. Geogr. Space 17, 169–190.

Temitopi, D., Oyedotun, T., 2014. Shoreline geometry: DSAS as a tool for historical trend analysis. J. Environ. Geogr. 7 (1-2), 2047, 0371.

Thakur, S., Mondal, I., Bar, I., Nandi, S., Ghosh, P.B., Das, P., De, T.K., 2020b. Shoreline changes and their impact on the mangrove ecosystems of some islands of Indian Sundarbans, North-East Coast of India. J. Clean. Prod. https://doi.org/10.1016/j.jclepro.2020.124764.

Thieler, E.R., Himmelstoss, E.A., Zichichi, J.L., & Ergul, A. (2009). *The Digital Shoreline Analysis System (DSAS) version 4.0—An ArcGIS extension for calculating shoreline change* (US Geological Survey Open-File Report 2008-1278). http://woodshole.er.usgs.gov/project-pages/dsas/version4.

Vu, M.T., Lacroix, Y., Than, V.V., Nguyen, V.T., 2020. Prediction of shoreline changes in Almanarre beach using geospatial techniques. Indian. J. Geo-Mar. Sci. 49, 207–217.

Williams, A., Rangel-Buitrago, N., Pranzini, E., Anfuso, G., 2018. The management of coastal erosion. Ocean. Coast. Manag. 156, 4. https://doi.org/10.1016/j.ocecoaman.2017.03.022.

Zhang, X., Yang, Z., Zhang, Y., Ji, Y., Wang, H., Lv, K., Lu, Z., 2017. Spatial and temporal shoreline changes of the southern Yellow River (Huanghe) Delta in 1976–2016. Mar. Geol. 395, 188–197. https://doi.org/10.1016/j.margeo.2017.10.006.